Eps15 and Dap160 control synaptic vesicle membrane retrieval and synapse development

Tong-Wey Koh,[1] Viktor I. Korolchuk,[5] Yogesh P. Wairkar,[5] Wei Jiao,[6] Emma Evergren,[6] Hongling Pan,[2] Yi Zhou,[2] Koen J.T. Venken,[1] Oleg Shupliakov,[6] Iain M. Robinson,[5,7] Cahir J. O'Kane,[5] and Hugo J. Bellen[1,2,3,4]

[1]Graduate Program in Developmental Biology, [2]Department of Molecular and Human Genetics, [3]Department of Neuroscience, and [4]Howard Hughes Medical Institute, Baylor College of Medicine, Houston, TX 77030
[5]Department of Genetics, University of Cambridge, Cambridge CB2 3EH, England, UK
[6]Department of Neuroscience, Karolinska Institutet, SE-171 77 Stockholm, Sweden
[7]Institute of Biomedical and Clinical Sciences, Peninsula College of Medicine and Dentistry, Plymouth PL6 8BU, England, UK

Epidermal growth factor receptor pathway substrate clone 15 (Eps15) is a protein implicated in endocytosis, endosomal protein sorting, and cytoskeletal organization. Its role is, however, still unclear, because of reasons including limitations of dominant-negative experiments and apparent redundancy with other endocytic proteins. We generated *Drosophila eps15*-null mutants and show that Eps15 is required for proper synaptic bouton development and normal levels of synaptic vesicle (SV) endocytosis. Consistent with a role in SV endocytosis, Eps15 moves from the center of synaptic boutons to the periphery in response to synaptic activity. The endocytic protein, Dap160/intersectin, is a major binding partner of Eps15, and *eps15* mutants phenotypically resemble *dap160* mutants. Analyses of *eps15 dap160* double mutants suggest that Eps15 functions in concert with Dap160 during SV endocytosis. Based on these data, we hypothesize that Eps15 and Dap160 promote the efficiency of endocytosis from the plasma membrane by maintaining high concentrations of multiple endocytic proteins, including dynamin, at synapses.

Introduction

Endocytosis is crucial for the reformation of functional synaptic vesicles (SVs) after exocytosis of neurotransmitters. Although multiple mechanisms have been observed during SV endocytosis (Gad et al., 2000; Teng and Wilkinson, 2000; Sun et al., 2002; Granseth et al., 2006; He et al., 2006), all of these involve the detachment of the vesicle from the plasma membrane, a step that is known as fission. Current evidence indicates that the GTPase dynamin functions at the fission step. For example, endocytic vesicles are arrested at the fission step in *shibire*^{ts1}, a temperature-sensitive mutant of dynamin, and in the presence of the nonhydrolyzable analogue of GTP (Kosaka and Ikeda, 1983; Takei et al., 1998). As inhibition of dynamin leads to complete blockage of SV endocytosis in *shibire* mutants, dynamin activity is absolutely required for SV endocytosis (Koenig and Ikeda, 1989; Shupliakov et al., 1997; Verstreken et al., 2002; Poskanzer et al., 2003).

To further understand dynamin function, we and others have previously characterized a major binding partner of dynamin, Dap160 (dynamin-associated protein 160 kD) and shown that it maintains proper dynamin localization at synapses (Broadie, 2004; Koh et al., 2004; Marie et al., 2004; Evergren et al., 2007). Although there is a complete block in endocytosis during inhibition of dynamin function, residual endocytic activity persists in the absence of Dap160. This prompted us to study other proteins that may function in conjunction with dynamin.

EGF receptor pathway kinase substrate clone 15 (Eps15) has been found in protein complexes with multiple endocytic proteins, including dynamin and the vertebrate homologue of Dap160, intersectin (Santolini et al., 1999; Sengar et al., 1999; Salcini et al., 2001). Originally discovered as an EGF receptor kinase

T.-W. Koh and V.I. Korolchuk contributed equally to this paper.

Correspondence to Cahir J. O'Kane: c.okane@gen.cam.ac.uk; or Hugo J. Bellen: hbellen@bcm.tmc.edu

T.-W. Koh's present address is Department of Molecular, Cellular, and Developmental Biology, Yale University, New Haven, CT 06511.

V.I. Koroluchuk's present address is School of Clinical Medicine, Cambridge Institute for Medical Research, Cambridge CB2 0XY, UK.

Y.P. Wairkar's present address is Department of Molecular Biology and Pharmacology, School of Medicine, Washington University in St. Louis, St. Louis, MO 63110.

Abbreviations used in this paper: Dap160, dynamin-associated protein 160 kD; EH, Eps15 homology; EJP, excitatory junctional potential; Eps15, EGF receptor pathway substrate clone 15; FRT, FLP recognition target; mEJP, miniature EJP; NMJ, neuromuscular junction; SV, synaptic vesicle; TEM, transmission EM; UIM, ubiquitin-interacting motif.

The online version of this article contains supplemental material.

The Journal of Cell Biology, Vol. 178, No. 2, July 16, 2007 309–322
http://www.jcb.org/cgi/doi/10.1083/jcb.200701030

substrate and a putative oncogene, Eps15 was later implicated in endocytosis and endosomal trafficking by in vitro studies (Fazioli et al., 1993; Tang and Cai, 1996; Tebar et al., 1996; Wendland et al., 1996; Carbone et al., 1997; Benmerah et al., 1999; Torrisi et al., 1999; Bache et al., 2003). Intriguingly, RNA interference knockdown of Eps15 in a nonneuronal cell line indicated that Eps15 is redundant with other endocytic proteins during the endocytosis of EGF receptor (Sigismund et al., 2005). This prompted several groups of investigators to examine its role in SV endocytosis. In *Caenorhabditis elegans*, *eps15*-null mutants undergo a temperature-sensitive paralysis, and mutant nerve terminals exhibit vesicle depletion at high temperatures, indicating a role for Eps15 in maintaining the presence of SVs at the nerve terminals (Salcini et al., 2001). More recently, a *Drosophila* mutant with reduced Eps15 levels was shown to undergo impairment in neurotransmission and paralysis only at high temperatures but not at physiological temperatures (Majumdar et al., 2006). In contrast, injection of dominant-negative peptides to inhibit Eps15 function in squid axonal terminals leads to a very subtle decrease in the number of SVs but a strong inhibition of neurotransmitter release (Morgan et al., 2003). The in vivo data therefore suggest that Eps15 plays either an accessory role or no role in endocytosis. We therefore decided to generate *eps15* protein-null alleles and investigate the role of Eps15 in flies in more detail.

Here, we describe the functional characterization of *Drosophila* Eps15 to address the following questions: (1) Does Eps15 function in endocytosis of SVs from the plasma membrane at the nerve terminal? (2) If so, at which step is Eps15 involved? (3) Is there a functional relationship between Eps15 and Dap160? Our data indicate that Eps15 is required for efficient SV endocytosis and that loss of Eps15 causes a very severe reduction in dynamin and Dap160 protein levels at neuromuscular junctions (NMJs). Furthermore, the endocytic defects of *eps15*- and *dap160*-null mutations are not additive, suggesting that Eps15 and Dap160 act at the same step during endocytosis.

Results

Drosophila eps15 is an essential gene

The *Drosophila* genome contains a single homologue of mammalian Eps15 (Lloyd et al., 2000). It has three Eps15 homology (EH) domains, a coiled coil domain, a region with multiple DPF (aspartate-proline-phenylalanine) motifs, and at least one, possibly two, ubiquitin-interacting motifs (UIMs) at the C terminus, similar to its mammalian homologue (Fig. S1 A, available at http://www.jcb.org/cgi/content/full/jcb.200701030/DC1; Polo et al., 2002). To determine its spatial and subcellular distribution, we raised two different polyclonal antibodies against epitopes shown in Fig. S1 A: a rabbit antibody and a guinea pig antibody. Both antibodies are specific, as mutants that lack the *eps15* gene display no immunoreactivity on Western blots (Fig. 1 D and Fig. S1 B) and immunohistochemically stained tissues (Fig. 2 A and Fig. S1, C and D). Western blots of fly heads show an ~160-kD and a 90-kD band, whereas the predicted mol wt is ~132 kD (Fig. 1 D). Immunoprecipitation experiments with rabbit anti-Eps15 and fly head protein extracts show that Eps15

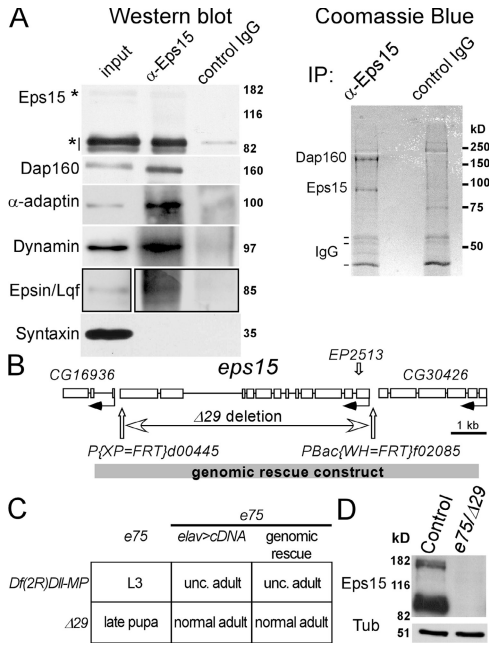

Figure 1. **Binding partners of *Drosophila* Eps15 and generation of two null alleles of fly *eps15*.** (A, left) Anti-Eps15 antiserum coimmunoprecipitates Eps15 with Dap160, α-adaptin, dynamin, and epsin/Lqf, but not Syntaxin (input is 5%). Asterisks mark the positions of Eps15-specific bands. (right) Coomassie staining shows that Dap160 is the major binding partner of Eps15 in the coimmunoprecipitate; bands were identified by mass spectroscopy (see Table S1, available at http://www.jcb.org/cgi/content/full/jcb.200701030/DC1, for peptide sequences). (B) The *eps15* genomic locus is tagged with three different transposable elements, *EP2513*, *P{XP=FRT}d00445*, and *PBac{WH=FRT}f02085*. *EP2513* was excised to generate an imprecise deletion allele $eps15^{e75}$ (*e75*). The *FRT* sites in *P{XP=FRT}d00445* and *PBac{WH=FRT}f02085* were used to generate an FLP-mediated site-specific deletion of the entire *eps15* coding region, resulting in the allele $eps15^{\Delta 29}$ (*Δ29*). The gray bar indicates the genomic region that was used to rescue the *eps15* mutants. This region contains the entire *eps15* locus and partial sequences of two flanking genes. (C) Lethal phase analysis of mutants in heteroallelic combinations and in the presence or absence of rescue constructs driven by $elav^{C155\text{-}Gal4}$ (see Materials and methods). (D) The $eps15^{e75}$ and $eps15^{\Delta 29}$ mutations cause loss of Eps15 protein expression as revealed by Western blot analysis using rabbit anti-Eps15. Each lane contains proteins extracted from 10 brains of $eps15^{e75}/eps15^{\Delta 29}$ (*e75/Δ29*) and *w* control larvae. See also Fig. S1 for Western blot and immunohistochemistry of homozygous *e75* larvae.

binds to Dap160, as detected by Western blot and mass spectrometry of Coomassie blue–stained bands (Fig. 1 A and Table S1). The Coomassie blue–stained gel indicates that Dap160 is a major binding partner of Eps15, in agreement with the biochemical interaction data for the vertebrate homologue of Dap160, intersectin (Sengar et al., 1999). In addition, rabbit anti-Eps15 also coimmunoprecipitates Eps15 with α-adaptin, epsin/Liquid facets, and dynamin (Fig. 1 A), consistent with protein interaction studies using the rat and *C. elegans* homologues of Eps15 (Benmerah et al., 1999; Salcini et al., 2001). In summary, *Drosophila* Eps15 shows structural and biochemical properties similar to Eps15 homologues in other organisms.

To determine the function of Eps15 in vivo, we disrupted the *eps15* gene using two different reverse genetic approaches. We imprecisely excised *EP2513*, a semilethal *P* element insertion in the 5′ untranslated region of the *eps15* gene (Fig. 1 B; Lloyd et al., 2000). This allowed isolation of a lethal allele, $eps15^{e75}$.

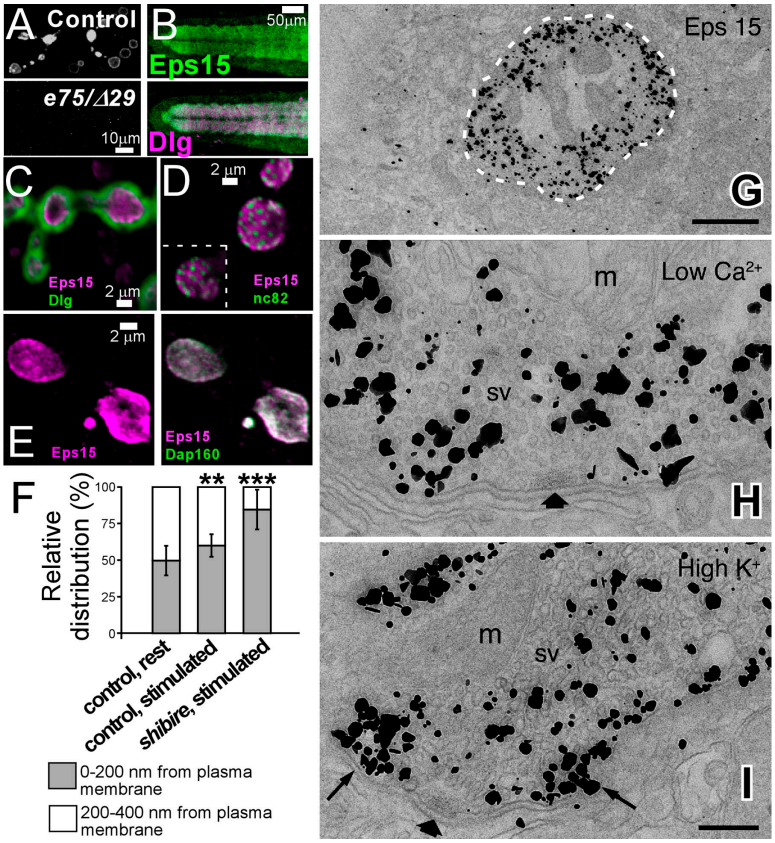

Figure 2. **Eps15 is enriched at synapses.** (A) Guinea pig anti-Eps15 detects Eps15 protein at the muscle 4 NMJ of a *w* control larva but not that of an *eps15*^{e75}/*eps15*$^{\Delta 29}$ mutant. (B) Eps15 (green) is closely associated with Dlg (magenta) in the neuropil of the larval ventral nerve cord. (bottom) Merge of anti-Eps15 and anti-Dlg staining patterns. (C) Dlg (green), which labels the postsynaptic compartment of the NMJ at this resolution, shows a pattern that envelopes that of Eps15 (magenta). This indicates that Eps15 is enriched in the presynaptic compartment at the NMJ. (D) Eps15 (magenta) is excluded from puncta decorated by Bruchpilot (nc82 antigen; green), which marks T-bars. (E) Eps15 (magenta; left) and Dap160 (green; right in merged panel) largely colocalize in the boutons, resulting in large areas of white in the merged image (right). A and C–E show single confocal slices, and B shows a projection view. (F) Eps15 immunogold labeling in two zones located within 500 nm lateral to T-bars (thick arrows in H and I). The first zone (gray bars) refers to areas 0–200 nm from the plasma membrane, and the second zone (white bars) refers to areas 200–400 nm from the plasma membrane. Relative distribution shows the percentage of total immunogold labeling distributed in either zones. Error bars indicate standard deviation. **, $P < 0.01$; ***, $P < 0.001$ (*t* test). Bar graphs represent mean values from 15 resting wild-type boutons, 18 wild-type boutons stimulated with 60 mM K^+, and 20 *shibire*^{ts1} boutons stimulated with 60 mM K^+. (G) Silver-enhanced immunogold labeling (black precipitates; see Materials and methods) of Eps15 using guinea pig anti-Eps15 reveals that Eps15 is associated with vesicle-rich regions of a wild-type resting bouton. (H) A high-magnification view of anti-Eps15 immunogold labeling in a wild-type resting bouton shows that Eps15 is associated with vesicles but largely excluded from the area around the synaptic dense body or T-bar (short wide arrow). (I) Upon stimulation with 60 mM K^+, anti-Eps15 immunogold labeling becomes concentrated at plasma membrane regions adjacent to the active zone (long arrows). Bars: (G) 1 μm; (H and I) 200 nm. Guinea pig anti-Eps15 was used in A, B, and E–I, and rabbit anti-Eps15 was used in C and D.

We also deleted the entire *eps15* locus by inducing site-specific recombination between two FLP recognition target (FRT)–containing transposons flanking the *eps15* locus, generating *eps15*$^{\Delta 29}$ (Fig. 1 B; Golic, 1994; Thibault et al., 2004). Complementation analysis revealed that *eps15*^{EP2513}, *eps15*^{e75}, *eps15*$^{\Delta 29}$, and *Df(2R)Dll-MP* (a large deficiency uncovering the genomic region encompassing the *eps15* locus), all fail to complement each other's lethality, indicating that each of these mutations affects the same gene, presumably *eps15* (Fig. 1 C). To determine the severity of these mutations, we examined the lethal phase of the mutants in various allelic combinations. The *eps15*$^{\Delta 29}$ homozygote and *eps15*^{e75}/*eps15*$^{\Delta 29}$ transheterozygote animals die as pharate adults, *eps15*^{e75} homozygous animals die as first instars, and *eps15*^{e75}/*Df(2R)Dll-MP* transheterozygotes die as third instars (Fig. 1 C). To ensure that the lethality is due to mutations in the *eps15* gene, we introduced a genomic fragment encompassing the *eps15* locus into the mutant backgrounds (Fig. 1 B; genomic rescue construct). This rescues *eps15*$^{\Delta 29}$ homozygotes and *eps15*^{e75}/*eps15*$^{\Delta 29}$ transheterozygotes to normal adults but only partially rescues *eps15*^{e75}/*Df(2R)Dll-MP* transheterozygotes, as the adults are uncoordinated. The lethal phase and the rescue data indicate that the lethality of *eps15*$^{\Delta 29}$ is solely due to deletion of the *eps15* locus and that *eps15*^{e75} carries a second site mutation that is not shared by *eps15*$^{\Delta 29}$. To determine whether Eps15 is required in the nervous system, we expressed the *eps15* cDNA using a neuronal-specific driver (*elav-Gal4*). This rescued *eps15*^{e75}/*eps15*$^{\Delta 29}$ to normal adults with no obvious morphological defects, indicating that Eps15 is predominantly required in the nervous system (Fig. 1 C).

To determine which mutations correspond to null alleles, we performed Western blot analyses. The *eps15*^{e75}/*eps15*^{e75} and *eps15*^{e75}/*eps15*$^{\Delta 29}$ animals do not express detectable levels of Eps15 protein on Western blots (Fig. 1 D and Fig. S1 B). In summary, we have isolated two independent protein-null mutations, *eps15*^{e75} and *eps15*$^{\Delta 29}$, which cause lethality, indicating that *eps15* is an essential gene in *Drosophila*, unlike the *C. elegans* *eps15*-null mutation, which is viable (Salcini et al., 2001). In addition, the essential role of Eps15 is confined to the nervous system in flies.

Eps15 is enriched at synapses in the SV pool and migrates to the plasma membrane during stimulation

To determine where Eps15 is expressed, we performed immunohistochemistry of third instar larvae (Bellen and Budnik, 2000). Both anti-Eps15 antibodies reveal the same expression profiles, and this immunoreactivity is lost in null mutant animals, indicating that the labeling is specific (Fig. 2 A and Fig. S1, C and D). Eps15 is expressed broadly in the nervous system and is much enriched in the neuropil of the central nervous system and at the NMJs (Fig. 2, A–I). In addition, most, and possibly all, imaginal discs also express Eps15 (unpublished data). To determine the subsynaptic localization of Eps15 at the NMJ, we costained Eps15 with Dlg, which at this resolution is effectively a postsynaptic

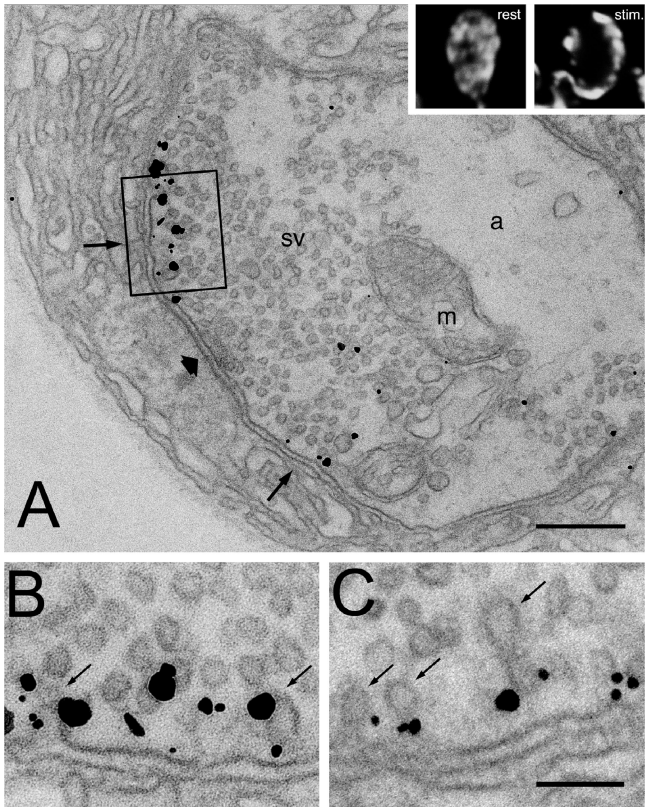

Figure 3. **High K^+ stimulation of *shibire*^{ts1} NMJs at the restrictive temperature leads to a dramatic redistribution of Eps15 in boutons independent of SVs.** (A) Silver-enhanced immunogold labeling of Eps15 using guinea pig anti-Eps15 reveals that Eps15 is predominantly localized to the plasma membrane (thin arrows) in areas surrounding the T-bars (thick arrow; the 60 mM K^+ stimulus did not completely deplete the preexisting pool of vesicles in the *shibire*^{ts1} bouton). As reported previously in *shibire*^{ts1} mutants, this stimulus leads to mild depletions of the vesicle pool in a subset of boutons (A) and more severe depletions in other boutons (not depicted), even though endocytosis is blocked at the restrictive temperature (Estes et al., 1996). (Inset) Confocal imaging of guinea pig anti-Eps15 staining reveals that Eps15 is localized in the lumen of a resting bouton (rest) and is redistributed to the periphery in a bouton stimulated with 60 mM K^+ (stim). m, mitochondria; a, axoplasm. (B) Boxed area in A is shown at higher magnification. (C) Electron micrograph of the same area from an adjacent ultrathin section. Gold particles were often located close to the rims of invaginating pits at the plasma membrane. Small arrows indicate fuzzy coats on vesicles. Although the areas that are immunolabeled for Eps15 seem to be reduced after stimulation, levels of Eps15 proteins are unchanged in resting and stimulated control and *shibire*^{ts1} terminals (quantification by immunofluorescent microscopy; not depicted). Bars: (A) 300 nm; (B and C) 100 nm.

marker (Lahey et al., 1994). Eps15 is enveloped by Dlg at the NMJ, indicating that Eps15 is enriched in the presynaptic compartment (Fig. 2 C). Collectively, we conclude that Eps15 is widely expressed but is enriched in the neuropil and in the presynaptic compartment of the NMJ.

At the NMJ, Eps15 is present in the central region of the boutons in a honeycomb-like pattern, where most Eps15 staining was found surrounding active zones, defined by anti-Bruchpilot/nc82 (Fig. 2 D; Wucherpfennig et al., 2003; Wagh et al., 2006). In addition, Eps15 shows extensive colocalization with Dap160 (Fig. 2 E). Therefore, at the level of confocal microscopy, Eps15 is enriched in areas surrounding active zones and colocalizes with Dap160, which has been reported to show a similar honeycomb-like localization pattern (Roos and Kelly, 1999). These data prompted us to investigate Eps15 localization at the ultrastructural level. Silver-enhanced immunogold labeling of resting wild-type NMJ boutons with anti-Eps15 reveals that Eps15 is associated with vesicles in the lumen of boutons but is at neither presynaptic dense bodies (T-bars) nor vesicle-free areas of the boutons (Fig. 2, G–H, black precipitates; see Materials and methods). This immunogold labeling pattern is not observed when a nonrelevant primary antibody was used, indicating that the anti-Eps15 label is specific (unpublished data). Upon a mild stimulation with 60 mM K^+, Eps15 becomes more concentrated in regions close to the plasma membrane surrounding the T-bars (Fig. 2, F and I). This redistribution of Eps15 is particularly evident in *shibire*^{ts1} mutants stimulated at a restrictive temperature (Fig. 2 F and Fig. 3 A). Interestingly, a subset of Eps15 is localized to the rim of invaginating vesicles or pits at the plasma membrane in stimulated *shibire*^{ts1} mutant boutons (Fig. 3, B and C). In summary, Eps15 is associated with vesicle in resting boutons and is mobilized to areas adjacent to active zones upon stimulation.

Eps15 regulates neuromuscular synapse development

A larval NMJ typically consists of a series of boutons connected by neurites, like beads on string. These boutons are dynamic structures that sprout and retract during larval development (Eaton et al., 2002). Because Dap160 mutants display numerous extra NMJ boutons and branching (Koh et al., 2004; Marie et al., 2004), and because Eps15 and Dap160 interact, we quantified the number of boutons and branches in *eps15* mutant NMJs. Compared with controls, mutant larvae show a pronounced increase in bouton number at three different NMJ synapses (Fig. 4, A–D and F). In addition, control NMJs typically have few branchpoints from which boutons sprout (Fig. 4, C and G, arrows). In contrast, *eps15* mutant NMJs show more branchpoints, some of which lead to more than two branches (Fig. 4, D and G). For example, mutant muscle 4 synapses commonly exhibit boutons with three branches or more, but such hyperbranched boutons are infrequent in controls (Fig. 4, C, D, and G). Thus, *eps15* mutant NMJs show supernumerary boutons and branches when compared with controls, similar to Dap160 mutants (Koh et al., 2004; Marie et al., 2004).

Eps15 is required to sustain high-frequency neurotransmitter release

Eps15 has been implicated in endocytosis and endosomal trafficking (Tebar et al., 1996; Benmerah et al., 1999; Torrisi et al., 1999; Bache et al., 2003). In addition, loss of Eps15 in *C. elegans* leads to a defect in vesicle cycling at the restrictive temperature (Salcini et al., 2001). To define the role of Eps15 in the SV cycle more precisely, we performed electrophysiological assays of mutant *eps15* NMJs. To determine whether the exocytic machinery is intact, we elicited low-frequency stimuli and recorded evoked excitatory junctional potentials (EJPs) in 0.5, 1, and 5 mM extracellular Ca^{2+}. Under these conditions, the EJPs are similar to wild-type amplitudes (Fig. 5 A). In addition, spontaneous release or miniature EJPs (mEJPs) of *eps15* mutants

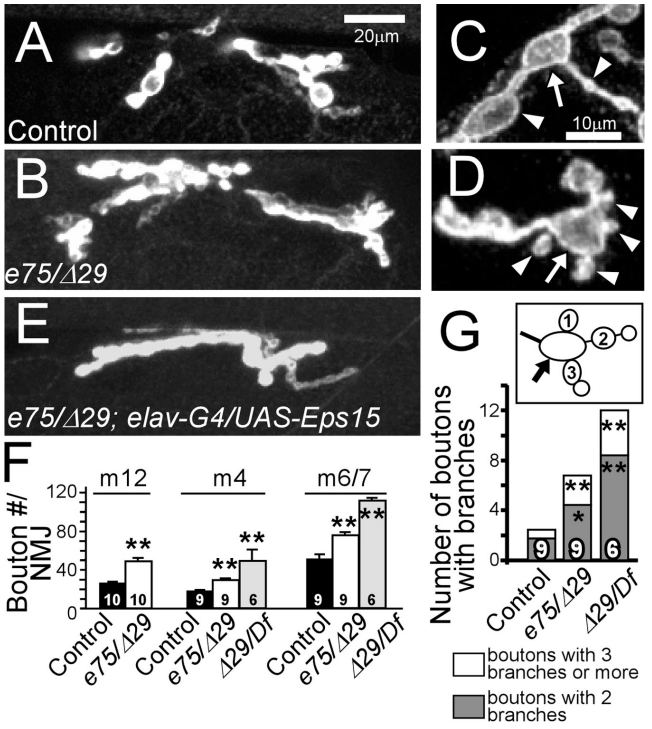

Figure 4. ***eps15* mutants show bouton overgrowth at the NMJ.** Muscle 12 NMJ of *eps15*^{e75}/*eps15*$^{\Delta 29}$ L3 larva (B) possess more boutons and branches than a control larva (A) as revealed by mouse anti-Dlg staining. A close-up view of anti-HRP–stained muscle 4 type IB boutons reveals that there are more branchpoints (arrows) in *eps15*^{e75}/*eps15*$^{\Delta 29}$ (D) than in controls (C). A bouton that was connected to more than one distal neurite or bouton (arrowheads) was counted as a branchpoint (arrow). (E) Neuronal expression of the full-length *eps15* cDNA rescues the supernumerary boutons at the muscle 12 in the *eps15*^{e75}/*eps15*$^{\Delta 29}$ background (see Fig. 9 B for quantification). (F) Comparison of mean bouton numbers per NMJ at muscle 12, 4, and 6/7 in *eps15*^{e75}/*eps15*$^{\Delta 29}$ (*e75/Δ29*), *eps15*$^{\Delta 29}$/*Df(2L)Dll-MP* (*Δ29/Df*), and control larvae reveals that *eps15* mutant NMJs possess significantly more boutons per synapse than control NMJs. In addition, bouton numbers at *Δ29/Df* NMJs are significantly more than those at *e75/Δ29* NMJs (m4, $P < 0.01$; m6/7, $P < 0.05$). (G) Comparison of branchpoint numbers per NMJ (arrow in inset shows an example of a bouton with three branches) reveals that *eps15* mutants muscle 4 NMJs possess more boutons with two branches (gray bar) and three or more branches (white bar) than controls. In addition, *Δ29/Df* NMJs exhibit somewhat more branchpoints than *e75/Δ29*, but the difference is not significant ($P > 0.05$). *w* larvae were used as controls. Bars: (A, B, and E) 20 μm; (C and D) 10 μm. *, $P < 0.05$; **, $P < 0.01$ (controls vs. mutants; Mann-Whitney U-test). Error bars indicate SEM, and the numbers in histograms indicate the number of larvae.

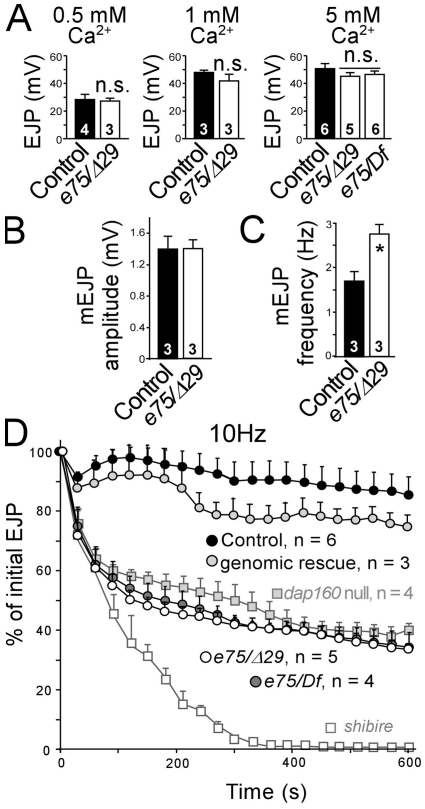

Figure 5. ***eps15* mutants show normal neurotransmitter release when stimulated at low frequency but are unable to sustain release under high-frequency stimulation.** (A) Mean EJP measured at the NMJ reveals that neurotransmitter release is normal at *eps15*^{e75}/*eps15*$^{\Delta 29}$ (*e75/Δ29*) and *eps15*^{e75}/*Df(2L)Dll-MP* (*e75/Df*) during 0.1 Hz of stimulation (0.5 and 1 mM Ca^{2+}) and single nerve stimulations (5 mM Ca^{2+}). (B) Mean mEJP amplitudes recorded in 0.5 mM Ca^{2+} and 3 μM tetrodotoxin were not different between *e75/Δ29* and *w* controls. (C) However, mean mEJP frequency of *e75/Δ29* is higher than controls. (D) When stimulated at 10 Hz, *eps15* mutant NMJs show defects in maintaining release. Specifically, the mean EJPs of both *e75/Δ29* and *e75/Df* were significantly different from controls ($P < 0.01$) after 60 s. Introducing one copy of *eps15* genomic fragment in the *e75/Δ29* background rescued this defect (genomic vs. control, $P > 0.1$; genomic vs. *e75/Δ29*, $P < 0.01$). Note that the two different *eps15*-null transheterozygotes show defects that are similar to that of *dap160*$^{\Delta 1}$/*Df(2L)bur-K1* (*dap160* null) but less severe than that of *shibire*^{ts1} (*shibire*^{ts1} data is adapted from Koh et al. [2004] for comparison). *w* larvae were used as controls. *, $P < 0.05$ (controls vs. mutants; Mann-Whitney U-test). Error bars indicate SEM, and the numbers in histograms indicate the number of larvae.

shows similar amplitude but higher frequency than controls (Fig. 5, B and C). Therefore, in the absence of Eps15, exocytosis of neurotransmitters is normal under low-frequency stimulation, but spontaneous release is altered.

To determine whether *eps15* mutant NMJs are able to efficiently recycle vesicles under repetitive stimulation, we applied 10 Hz of stimulation for 10 min in 5 mM extracellular Ca^{2+}. Control NMJs are able to maintain EJPs at ~90% of the initial amplitudes, but *eps15* NMJs show a strong synaptic depression to <40% of initial EJP amplitudes (Fig. 5 D). In this assay, *shibire*^{ts1}, encoding a temperature-sensitive dynamin mutant, depresses to zero as a result of a complete block in endocytosis, whereas *dap160* mutant NMJs show profiles of synaptic depression similar to those of *eps15* mutant NMJs (Fig. 5 D; Koh et al., 2004). Hence, *eps15* mutant NMJs show a defect in vesicle recycling that is similar to *dap160* mutant NMJs. Compared with our current data on *eps15* and *dap160* mutants, other endocytic mutants like *shibire*, *synaptojanin*, or *endophilin* show faster synaptic depression under a milder stimulation condition (higher Mg^{2+}/Ca^{2+} ratio) in our previous experiments (Verstreken et al., 2002). In summary, although exocytosis of neurotransmitters is essentially normal at *eps15* mutant NMJs, vesicle recycling is impaired but not blocked.

Eps15 is required for efficient SV endocytosis

One possible cause for the vesicle recycling defect in *eps15* mutants is impaired endocytosis. To assay for endocytosis at

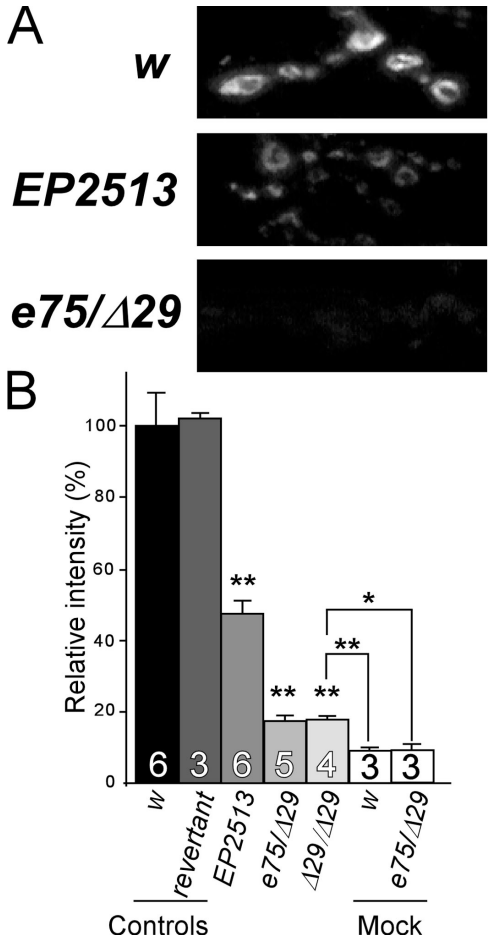

Figure 6. ***eps15* loss-of-function mutants show impaired FM1-43FX uptake during nerve stimulation.** (A) FM1-43FX, a lipophilic fluorescent dye was applied to the NMJ during stimulation with 90 mM K^+ and 5 mM Ca^{2+}. The "mock" control was performed by incubating the NMJ in FM1-43FX dissolved in a Ca^{2+}-free, low-K^+ medium. (B) FM1-43FX uptake expressed as the mean fluorescence intensity relative to *w* controls. The NMJ of L3 larvae homozygous for the hypomorphic allele *EP2513* show a mildly reduced dye uptake and that of the $eps15^{e75}/eps15^{\Delta 29}$-null mutants shows severely reduced dye uptake. In our hands, *EP2513* retains considerable levels of endocytic activities, which contrasts with the observation of little or no dye uptake in a recent characterization of the same allele (Majumdar et al., 2006). *, $P < 0.05$; **: $P < 0.01$ (controls vs. mutants; Mann-Whitney U-test). Error bars indicate SEM, and the numbers in histograms indicate the number of larvae.

the NMJs, we performed dye uptake experiments by applying a strong stimulus of 90 mM K^+ and 5 mM Ca^{2+} in the presence of the styryl dye FM1-43FX. Compared with controls, ~50% of dye uptake remains in the partial loss-of-function mutant $eps15^{EP2513}/eps15^{EP2513}$, whereas only ~20% of dye uptake remains in the *eps15*-null mutants, $eps15^{e75}/eps15^{\Delta 29}$ and $eps15^{\Delta 29}/eps15^{\Delta 29}$ (Fig. 6). To determine the background fluorescence level, we performed mock-labeling control experiments in which control and mutant NMJs were incubated with FM1-43FX in a Ca^{2+}-free/low-K^+ solution. Comparison with mock-labeled controls indicates that very low levels of dye uptake occur in the *eps15*-null mutants. The severe reduction in dye uptake phenotype in the *eps15*-null mutant can be rescued with neuronal expression of the *eps15* cDNA (see Fig. 9 C). In contrast to its role at the synapse, Eps15 is not essential for receptor-mediated endocytosis in hemocytes (Fig. S2, A–C and F, available at http://www.jcb.org/cgi/content/full/jcb.200701030/DC1) and in the *Drosophila* S2 cell line (RNAi knockdown experiment; unpublished data). Therefore, Eps15 is required for efficient SV endocytosis during nerve stimulation.

Endocytosis from the plasma membrane consists of sequential steps that can be observed with transmission EM (TEM). To further investigate the endocytic defect in *eps15* mutants, we quantified vesicle density and size of boutons in the resting state, during a strong stimulation with 90 mM K^+, and recovery after stimulation (Fig. 7, A–F). The vesicle densities of *eps15* mutant boutons at rest are not significantly different from those of controls (Fig. 7 A, B, and G; $P > 0.05$), in agreement with a lack of defect in exocytosis. Although the majority of vesicles in both control and *eps15* mutant boutons are <45 nm in diameter, we observe an increased proportion of abnormally large vesicles or cisternae in resting mutant boutons (Fig. 7, A, B, and H).

Because intense stimulations reveal reduced FM1-43FX uptake and more severe synaptic depression at *eps15* NMJs compared with controls, we applied 90 mM K^+ stimulation to control and *eps15* mutant boutons before processing for TEM. As shown in Fig. 7 (C, D, and G), we observed a reduction in vesicle densities in *eps15* mutant boutons when compared with control boutons. When allowed to recover for 1 min without stimulation, the vesicle densities in wild-type control boutons return to levels that are not significantly different from resting levels, but vesicle densities in *eps15* mutant boutons show a poor recovery (Fig. 7, E–G; $P > 0.05$). Relative to control boutons, the proportion of cisternae >85 nm is increased by stimulation in *eps15* mutant boutons but is reduced and returns to wild-type levels after a 1-min recovery (Fig. 7, I–K). In stimulated *eps15* mutant boutons, some cisternae appear to be large invaginations, which are contiguous with the plasma membrane (Fig. 7, K and L). In summary, *eps15* mutant boutons undergo vesicle depletion, accumulation of cisternae, and large membrane invaginations during stimulation. After 1 min of recovery, the relative size distributions of vesicles in *eps15* mutant and control boutons become similar, but the control boutons still have approximately twice the number of vesicles observed in mutant boutons. Thus, the TEM data indicate that Eps15 is required for efficient vesicle retrieval during intense stimulation. In its absence, bulk membrane invagination is not abolished, but budding of small clear vesicles from the plasma membrane and cisternae occur with much lower efficiency than in wild-type synapses.

The presence of large cisternae in *eps15* mutant boutons is reminiscent of *dap160* mutant boutons after a 1-min recovery from stimulation (Koh et al., 2004). This prompted us to examine *dap160* mutant bouton morphology during stimulation in more detail. As seen in *eps15* mutants, we observe cisternae and large membraneous bodies that appear to be contiguous to the plasma membrane (Fig. 7, M and N). The similarity of the large membrane invaginations in *eps15* and *dap160* mutant boutons suggests that both Eps15 and Dap160 act at a similar step in endocytosis.

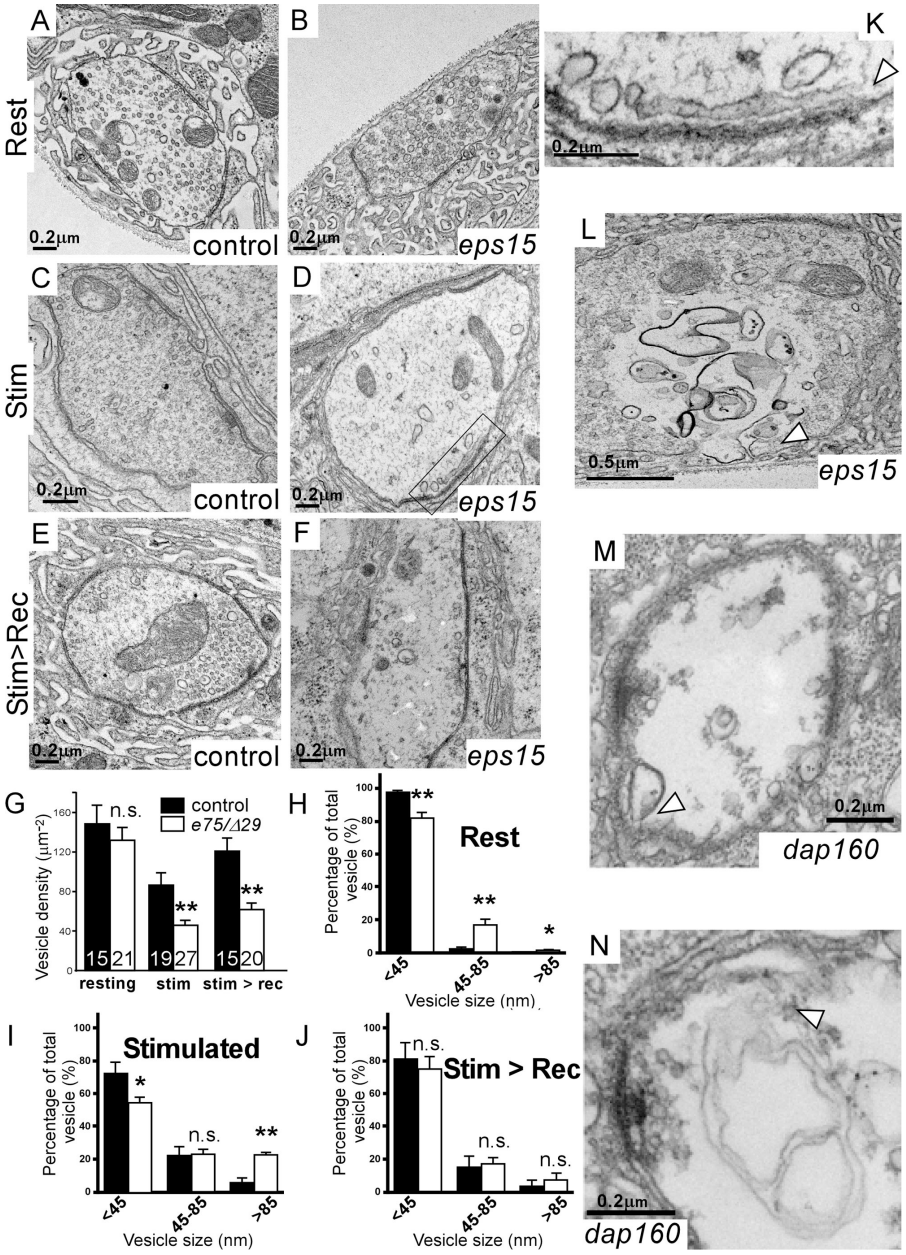

Figure 7. **TEM reveals a membrane retrieval defect at *eps15* mutant NMJs.** Compared with *w* controls (A), *eps15*^{e75}/*eps15*$^{\Delta 29}$ (*e75/Δ29*) mutants (B) have normal numbers of vesicles at rest but are inefficient in vesicle budding during endocytosis when stimulated with 90 mM K^+/5 mM Ca^{2+} (C, control; D, *e75/Δ29*). Upon incubation in normal HL3 without Ca^{2+} for 1 min, vesicle density recovers to near normal levels in controls (E) but not mutants (F). (G) Mean vesicle density in boutons at rest, after stimulation and recovery. Compared with controls, *e75/Δ29* mutant NMJs are much less efficient in the recovery of vesicles during stimulation. Vesicle densities of resting *e75/Δ29* and control boutons are not significantly different ($P > 0.05$). However, vesicle densities of *e75/Δ29* boutons during stimulation and after recovery are less than controls. Mean size distribution of vesicles at rest (H) and after stimulation (I) and recovery (J). *e75/Δ29* NMJ boutons accumulate a greater proportion of large membraneous bodies or cisternae during stimulation. (K) A high-magnification view of the boxed area in D shows a cisterna that appears to emanate from the plasma membrane (arrowhead). (L) Another mutant bouton showing large membraneous bodies (arrowheads) are apparently contiguous with the plasma membrane. Similarly, cisternae (M) and membrane invaginations (N) are seen in *dap160*$^{\Delta 1}$/*Df(2L)bur-K1* mutants when stimulated with 60 mM K^+ at 34°C. Vesicle quantification was performed on at least 15 boutons using two or three larvae per genotype for each condition. Vesicle size distribution was quantified using 300–800 vesicles for each genotype and condition. *, $P < 0.05$; **, $P < 0.01$ (controls vs. mutants; *t* test). Error bars indicate SEM, and the numbers in histograms indicate the number of boutons examined.

Eps15 maintains proper levels of dynamin and Dap160 at NMJs

The endocytic defects, in particular, the retrieval defects observed by TEM in *eps15* mutants resemble those observed in *dap160* mutants (Koh et al., 2004; Marie et al., 2004; Fig. 7, K–N) and are quite different from those associated with the loss of *endophilin* and *synaptojanin* (Verstreken et al., 2002, 2003). This suggests that Eps15 may be functionally related to Dap160, prompting us to examine the localization of Dap160 and its partner dynamin (Roos and Kelly, 1998), as well as other synaptic proteins in *eps15* mutant NMJs. Immunohistochemistry of *eps15* mutant NMJs shows that dynamin and Dap160 levels are severely reduced to ~10 and ~25% of control levels, respectively (Fig. 8 A). In addition, we observe reductions of other proteins associated with SV cycling, including Stoned B, synaptotagmin I, α-adaptin, and endophilin (Fig. 8 B; Littleton et al., 1993; Andrews et al., 1996; González-Gaitán and Jäckle, 1997; Verstreken et al., 2002). Cysteine string protein (Csp), a cochaperone protein required for proper neurotransmitter release, and Fas II, a cell-adhesion molecule implicated in synapse formation and function, are not significantly reduced at *eps15* mutant NMJs (Fig. 8 C; Zinsmaier et al., 1994; Schuster et al., 1996; $P > 0.05$). The strong reduction of Dap160 at *eps15* NMJs prompted us also to examine the Eps15 levels at *dap160* mutant NMJs. Although Eps15 levels are variably affected in different boutons and synapses, there is only a slight reduction, which is not statistically significant (Fig. 8 D; $P > 0.05$). These data indicate that Eps15 maintains normal levels of multiple synaptic proteins at the synapse.

The severe reductions of dynamin and Dap160 at *eps15* mutant NMJs suggest that these two proteins are critical partners of Eps15 in endocytosis. We then asked whether the reductions

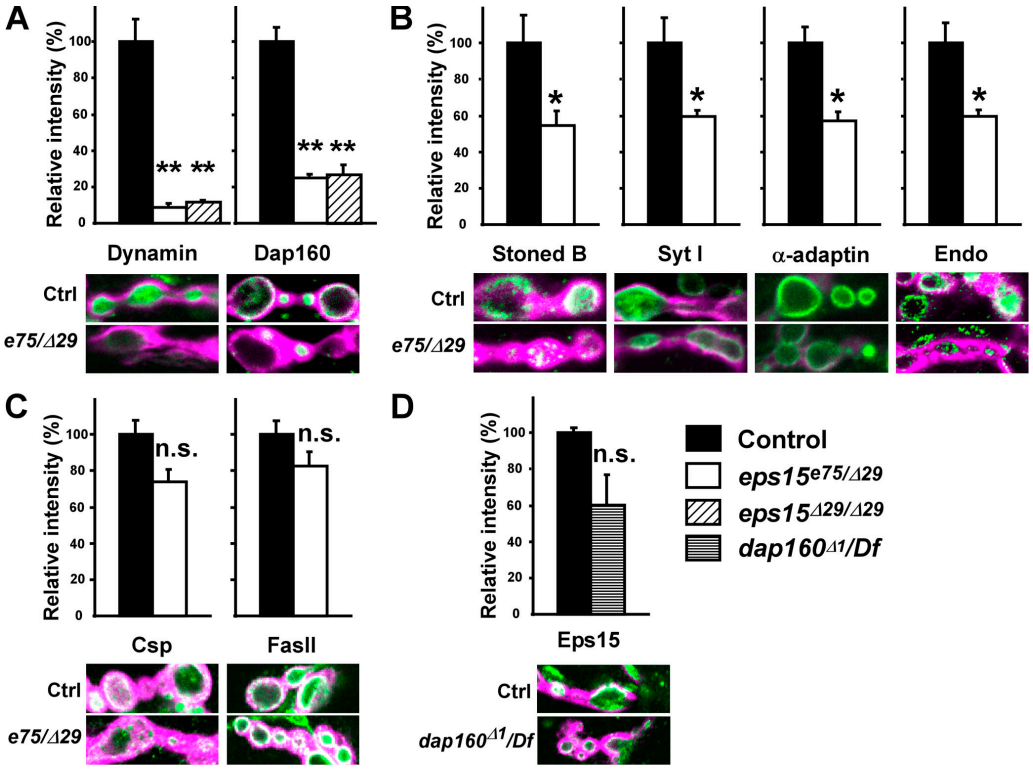

Figure 8. **Synaptic markers are reduced at *eps15* mutant NMJs.** Anti-Dlg outlines the NMJ boutons (magenta). The synaptic markers stained in green are quantified. (A) Dynamin and Dap160 are strongly reduced at *eps15* mutant NMJs. (B) Stoned B, synaptotagmin I, α-adaptin, and endophilin are mildly reduced. (C) Csp and FasII are not significantly reduced at the *eps15* mutant NMJs ($P > 0.05$). (D) Eps15 level is slightly but not significantly reduced at $dap160^{\Delta 1}/Df(2L)bur\text{-}K1$ NMJs compared with controls ($P > 0.05$). *w* larvae were used as controls. At least 10 muscle 12 type I boutons from abdominal segment 3 of each larva were used to obtain a pixel intensity for each larva, and at least three larvae were used to arrive at mean values for statistical comparisons. *, $P < 0.05$; **, $P < 0.01$ (controls vs. mutants; *t* test). Error bars indicate SEM.

of these two proteins are restricted to the synapse. Western blots of third instar larval brains indicate a subtle reduction of Dap160 levels and normal dynamin levels in the central nervous system (Fig. S3, available at http://www.jcb.org/cgi/content/full/jcb.200701030/DC1), suggesting that the reductions of these two proteins in *eps15* mutants occur predominantly at the synapse.

The C-terminal domains of Eps15 are not essential for SV endocytosis and synapse development

Because Eps15 possesses different domains that biochemically interact with various protein partners, it is possible that different domains are involved in distinct processes. To address this possibility, we verified the binding properties of three major protein–protein interaction domains of Eps15 using in vitro binding assays. Consistent with similar studies on the mammalian Eps15, the EH-, DPF- and the UIM-containing regions of *Drosophila* Eps15 bind Dap160, α-adaptin, and ubiquitin, respectively (Fig. S4, available at http://www.jcb.org/cgi/content/full/jcb.200701030/DC1; Benmerah et al., 1998; Sengar et al., 1999; Polo et al., 2002). We then tested the requirement of N- and C-terminal domains of Eps15 in SV endocytosis and synaptic bouton development by neuronally expressing three *eps15* cDNA constructs in the *eps15*-null background: (1) a full-length *eps15* cDNA (Eps15wt), (2) a truncated cDNA encoding only the N-terminal EH domains and coiled coil domains (ΔDPF; Fig. S1 A), and (3) a full-length cDNA with point mutations in the EH domains (EHmut; unpublished data). It is expected that the ΔDPF truncation protein will lose the ability to interact with α-adaptin and ubiquitinated proteins, whereas the EHmut protein will only lose the ability to bind Dap160 and other EH binding proteins (Benmerah et al., 1999; Santolini et al., 1999). EHmut is expressed but fails to localize at the NMJ and was not further analyzed (unpublished data). Eps15wt and ΔDPF are expressed and localized normally at the NMJ and rescue $eps15^{e75}/eps15^{\Delta 29}$ to normal adults (unpublished data). This allowed us to assess the function of ΔDPF at the NMJ with respect to synaptic bouton development and SV endocytosis.

To determine the contributions of Eps15 domains to synaptic bouton development, we quantified bouton numbers of the muscle 6/7 synapses (Fig. 9 B). The *eps15*-null mutants show approximately twice the number of NMJ boutons compared with controls. The supernumerary bouton phenotype is rescued by neuronal expression of Eps15wt and partially rescued by ΔDPF. Thus, the Eps15 C-terminal domains play minor roles in synaptic development.

Given the importance of α-adaptin in endocytosis, we asked whether a truncated Eps15 protein without the α-adaptin binding motifs can function normally in SV endocytosis by performing an FM1-43FX uptake assay. We observed rescue of the FM1-43FX uptake in *eps15*-null mutants by neuronal expression of Eps15wt and ΔDPF (Fig. 9 C). Interestingly, neuronal

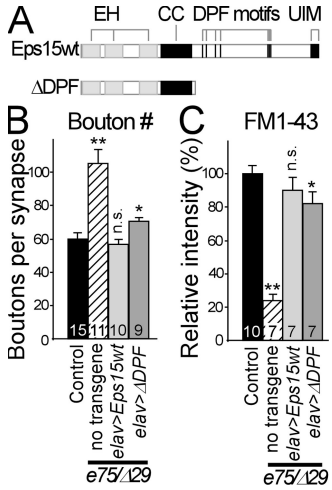

Figure 9. **An N-terminal fragment of Eps15 plays a major role in NMJ development and SV endocytosis.** (A) The ΔDPF truncation mutant of Eps15 contains the three EH domains and the coiled coil (CC) domain but lacks the C-terminal regions containing the DPF motifs (vertical black bars) and the UIMs. (B) Mean bouton numbers per synapse at muscle 6/7 synapses in control (revertant), *eps15*^{e75}/eps15$^{\Delta 29}$ (*e75/Δ29*), and *e75/Δ29* larvae expressing Eps15wt and ΔDPF. (C) Mean values of FM1-43FX uptake levels in *e75/Δ29* and *e75/Δ29* larvae expressing Eps15wt and ΔDPF relative to levels in control larvae (revertant). Expression of Eps15wt and ΔDPF are driven by *elav*$^{C155\text{-}Gal4}$ in B and by *elav-Gal4*^{3A4} in C. *, $P < 0.05$; **, $P < 0.01$ (controls vs. mutants; *t* test). Error bars indicate SEM, and the numbers in histograms indicate the number of larvae.

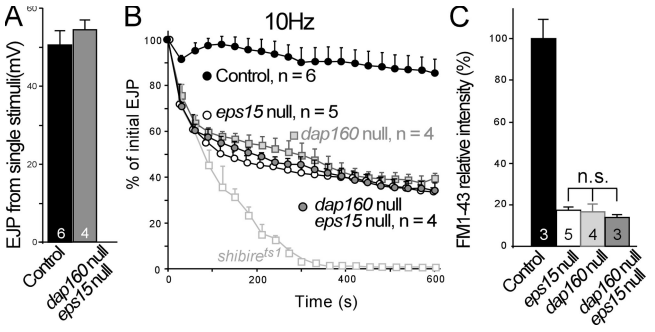

Figure 10. **Eps15 is a functional binding partner of Dap160.** (A) With single stimuli at 5 mM Ca^{2+}, *dap160*$^{\Delta 1}$ *eps15*^{e75}/*Df(2L)bur-K1* eps15$^{\Delta 29}$ double mutants (*dap160* and *eps15* null) show normal EJP. (B) When stimulated at 10 Hz in 5 mM Ca^{2+}, *dap160*- and *eps15*-null double mutants show synaptic depression kinetics that overlap with *eps15*^{e75}/eps15$^{\Delta 29}$ (*eps15* null) and *dap160*$^{\Delta 1}$/*Df(2L)bur*-K1(*dap160* null) single mutants. (*shibire*^{ts1} 34°C recordings are taken from Koh et al. [2004] for comparison.) (C) *dap160*- and *eps15*-null double mutants show reductions in FM1-43FX uptake similar to *eps15*- and *dap160*-null single mutants. *w* adults or larvae were used as controls. Error bars indicate SEM, and the numbers in histograms indicate the number of larvae.

expression of ΔDPF in *eps15*-null mutants show rescue of FM1-43FX uptake to a level significantly less than, but close to, control levels ($P < 0.05$). Therefore, the DPF-containing region plays a minor role in SV endocytosis. In summary, the roles of Eps15 in synaptic bouton development and SV endocytosis can be partially substituted by an N-terminal fragment containing the EH and coiled coil domains.

Eps15 and Dap160 function at the same endocytic step

Several observations suggest a functional relationship between Eps15 and Dap160. First, Eps15 and Dap160 physically bind to each other and colocalize at NMJs (Fig. 1 A and Fig. 2 E and Fig. S4 A; Sengar et al., 1999). Second, *eps15* mutant NMJs, like *dap160* mutant NMJs show extra boutons and branches (Fig. 4; Koh et al., 2004; Marie et al., 2004). Third, both *eps15* and *dap160* mutants exhibit endocytic defects but no exocytic defects at the NMJ (Figs. 5 and 6). Fourth, we observe large membraneous bodies in stimulated *eps15* and *dap160* mutant boutons (Koh et al., 2004; Fig. 7 K–N), which suggest a defect in the resolution of these large invaginations into small clear vesicles. Fifth, we observe a reduction of Dap160 levels at *eps15* mutant NMJs. These data suggest that the two proteins may function at very similar steps in endocytosis, namely, during vesicle budding from the plasma membrane and from large invaginations during bulk endocytosis. Because Dap160 and Eps15 share N-terminal EH domains, which are more homologous to each other than EH domains of other *Drosophila* proteins (40–60% similarity), it is possible that the EH domains of these two proteins serve redundant roles and act in parallel during endocytosis; if so, genetic ablation of both *eps15* and *dap160* should lead to more severe defects than either mutant alone. Alternatively, if Eps15 and Dap160 function at the same step during endocytosis from the plasma membrane, double-null mutants should have a phenotype similar to the single mutants.

To investigate the functional relationship between Eps15 and Dap160, we determined the endocytic defects of *eps15* and *dap160* mutants in double mutant larvae. First, we examined the lethal phases of double mutants and show that *dap160*- and *eps15*-null mutants live to pharate adult stage, similar to the single *eps15*- and *dap160*-null mutants. Second, *dap160*- and *eps15*-null mutants show normal evoked EJPs in response to single stimuli and during 10 Hz of stimulation; hence, these double mutants also show the same depression kinetics as the *eps15*- and *dap160*-null single mutants (Fig. 10, A and B). Thus, the loss of Dap160 does not enhance the endocytic defects in *eps15* mutants. To provide further support for the electrophysiology data, we performed FM1-43FX dye uptake experiments. As shown in Fig. 10 C, we observed a reduction in dye uptake in the double-null mutant that is similar to that of *eps15* and *dap160* single mutants. Thus, the *dap160*-null mutation does not affect the residual vesicle recycling in the *eps15*-null mutant background. In summary, these data argue that Eps15 and Dap160 act at the same step in SV endocytosis.

Discussion

Eps15 stabilizes multiple proteins in the presynaptic compartment

eps15 mutant NMJs exhibit a severe reduction in dynamin and Dap160 protein levels, suggesting a functional relationship between these proteins and Eps15. At the same time, we observe relatively mild reductions of α-adaptin, Stoned B, synaptotagmin I, and endophilin. The reduction of protein levels of dynamin, Dap160/intersectin, α-adaptin, and Stoned B in *eps15* mutants may be accountable by the interaction of these proteins

with Eps15 (Benmerah et al., 1999; Sengar et al., 1999; Martina et al., 2001; Salcini et al., 2001; Fig. 1 A). As our data suggest that Eps15 is not required to regulate global protein levels of dynamin and Dap160 (Fig. S3), Eps15 may facilitate anterograde axonal transport of dynamin and Dap160 through interaction of the EH domains with vesicular membrane proteins containing NPF motifs (Fernandez-Chacon et al., 2000). Alternatively, because Eps15 has been implicated in the endocytosis of synaptotagmin I (Jarousse et al., 2003), Eps15 may retain high concentrations of synaptic proteins by promoting the local recycling and sorting of vesicle-/membrane-associated proteins at synapses. Interestingly, a similar role has been proposed for Stoned in recycling synaptotagmin I at the synapse (Fergestad and Broadie, 2001; Diril et al., 2006).

Eps15 and Dap160 are required to maintain proper levels of dynamin at the NMJ

The endocytic defect in *eps15* can be largely ascribed to impaired vesicle budding from plasma membrane and cisternae. Compared with control boutons, stimulations of *eps15* mutant boutons result in more severe vesicle depletions, concurrent with the appearance of cisternae and large invaginations, which appear to be contiguous with the plasma membrane (Fig. 7, K and L). Importantly, 1 min after stimulation, wild-type control boutons recover to near normal vesicle densities, whereas *eps15* mutant boutons show little recovery. Note that internalization of cisternae, an early step in bulk endocytosis (Teng and Wilkinson, 2000; Royle and Lagnado, 2003), does occur in the mutants, but the cisternae are not efficiently resolved into properly sized SVs.

The endocytic intermediates found in *eps15* mutants resemble those observed when dynamin or Dap160 function is perturbed. Cisternae and invaginations contiguous with the plasma membrane have been reported at neuronal synapses during genetic or dominant-negative peptide perturbations of dynamin function in *Drosophila* and lampreys, respectively (Kosaka and Ikeda, 1983; Koenig and Ikeda, 1989, 1996, 1999; Koenig et al., 1993; Shupliakov et al., 1997). We have previously reported that *dap160* mutant NMJs show accumulation of cisternae during recovery from stimulation (Koh et al., 2004). Here, we fixed *dap160* mutants during stimulation and observed severe vesicle depletion concurrent with large invaginations from the plasma membrane, similar to those observed in *eps15*. Because dynamin levels are severely reduced at *eps15* and *dap160* NMJs, it is likely that both Eps15 and Dap160 act in concert to maintain high concentrations of dynamin at the synapse. Indeed, *dap160 eps15* double mutants show the same defects in dye uptake and in maintaining release during prolonged stimulations as the *eps15* and *dap160* single mutants, suggesting that both Eps15 and Dap160 act at the same step in endocytosis. Furthermore, the notion that Eps15 is localized at the site of dynamin action is consistent with the mobilization of Eps15 to the plasma membrane in the vicinity of endocytic intermediates in stimulated nerve terminals (Figs. 2 and 3). In addition, a functional interaction between Eps15 and dynamin is further bolstered by the recent demonstration of genetic interaction between *shibire* mutants and the hypomorphic *eps15* mutant, $eps15^{EP2513}$ (Majumdar et al., 2006). Note that the lack of endocytic defect in *eps15* mutant hemocytes also correlates with normal dynamin levels in these cells (Fig. S2), further corroborating with a link between SV endocytosis and the Eps15–Dap160–dynamin interaction. In agreement with the correlation of endocytic defects with reduced dynamin levels in *eps15* and *dap160* mutants, the GTPase activity of dynamin is allosterically dependent on dynamin protein concentration (Stowell et al., 1999). Therefore, these data suggest that the maintenance of high dynamin levels at synapses is one of the key functions of Eps15 and Dap160 in SV endocytosis.

Although we observed severe reduction of dynamin levels in both *eps15* and *dap160* mutants, there are subtle differences in synaptic protein levels between *eps15* and *dap160* mutants. For example, there is a reduction of synaptotagmin I in *eps15* mutants, which was not observed in *dap160* mutants. This may have resulted in minor differences in phenotypes, such as an increase in mEJP amplitudes in *dap160* mutants but not in *eps15* mutants.

Eps15 has been implicated in clathrin-coated pit assembly in nonneuronal cells, based on its interaction with α-adaptin (Tebar et al., 1996; Carbone et al., 1997; Benmerah et al., 1999; Torrisi et al., 1999). However, our data indicate that a truncated Eps15 protein lacking the α-adaptin–interacting DPF motifs (ΔDPF) partially rescues the FM1-43FX uptake defect of the *eps15*-null mutant. This suggests that a direct interaction between Eps15 and α-adaptin is not essential for SV endocytosis. Consistent with the nonessential role of the DPF domain of Eps15, the Eps15 binding region of α-adaptin is not essential for the rescue of transferrin endocytosis after α-adaptin siRNA knockdown (Motley et al., 2006). Hence, we propose that the dynamin–Dap160–Eps15 interaction is important for SV endocytosis.

A model of Eps15 function during SV endocytosis and synapse development

Based on our data and previous work, we propose a two-tier model for Eps15 function during SV endocytosis and synapse development. During SV endocytosis, Eps15 and Dap160 act together to stabilize several proteins at the synapse. In particular, the Eps15–Dap160 complex maintains high concentrations of dynamin, allowing allosteric activation of its GTPase activity, which is crucial for the resolution of newly internalized membranes into SVs (Stowell et al., 1999). It has been proposed that actin polymerization propels endocytosed vesicles toward the interior of the cell during dynamin-mediated endocytosis (Merrifield et al., 2002; Shupliakov et al., 2002; Itoh et al., 2005; Tsujita et al., 2006). Given that Eps15, Dap160, and related EH domain proteins in yeast have been implicated in regulating the actin cytoskeleton (Tang and Cai, 1996; Duncan et al., 2001; Zamanian and Kelly, 2003; Koh et al., 2004; Marie et al., 2004), it is tempting to speculate that the Eps15–Dap160 complex functions as a molecular scaffold to coordinate dynamin function in SV endocytosis with actin polymerization, a role that has been previously proposed for Dap160 (McPherson, 2002). It is thus interesting that the redistribution of Eps15 and Dap160 within NMJ boutons during stimulation suggests a dynamic role

of Eps15 and Dap160 during endocytosis (Fig. 2, F–I; and Fig. 3 A; Roos and Kelly, 1998, 1999).

In addition to its role in SV endocytosis, Eps15 may function in concert with Dap160 during synapse development through regulation of signal transduction pathways and/or cytoskeletal organization. Both Eps15 and Dap160 have been implicated in signal transduction pathways (Irie and Yamaguchi, 2002; Polo et al., 2003). In addition, Dap160/intersectin has been proposed to regulate cytoskeletal organization at the *Drosophila* NMJ and in mammalian cells through interaction with actin-associated molecules like WASp (Zamanian and Kelly, 2003; Koh et al., 2004; Marie et al., 2004). This is consistent with our recent data on lamprey reticulospinal synapses, which show that actin at synaptic endocytic sties is reorganized when intersectin interactions are perturbed (Evergren et al., 2007). Interestingly, an EH domain protein is involved in cytoskeletal reorganization during budding of yeast cells (Tang and Cai, 1996; Duncan et al., 2001), which is thought to be analogous to *Drosophila* NMJ bouton formation (Pennetta et al., 2002). We speculate that Eps15 and Dap160 may function as a protein complex—with Nervous wreck and WASp—that regulates cytoskeletal organization during synapse development (Coyle et al., 2004; Koh et al., 2004; Marie et al., 2004). In this respect, Eps15 and Dap160 may serve to bridge upstream signal transduction pathways and cytoskeletal organization during synapse development.

Materials and methods

Antibody generation

Two fragments encoding amino acid residues 586–816 and 915–1093 from Eps15 cDNA (SD09478 from Research Genetics) were cloned into the pGEX4T1 expression vector in frame with the GST coding region. GST-Eps15 (586–816) was used to generate the rabbit polyclonal antiserum, Rb Ab, and GST-Eps15 (915–1093) was used to generate guinea pig polyclonal antiserum, Gp Ab.

Fly genetics

***P* element excisions.** *w; EP(2)2513* (Rørth, 1996) was crossed to y^1 *w*; CyO, H{*w^{+mC}*=PΔ2-3}HoP2.1/Bc*^{1} *Egfr*^{F1} (Gerlitz et al., 2002) to generate 810 independent excision lines. Lines that failed to complement Df(2R)Dll-MP (Cohen et al., 1989) were characterized. Excisions were balanced over *CyO, P{*w^{+mC}*=Gal4-twi.G} P{*w^{+mC}*=UAS-2xEGFP}* (Halfon et al., 2002), and immunohistochemistry and Western blot were performed to identify allele $eps15^{e75}$. Remnants of the P element are still inserted in its original genomic location, but the exact lesion is not known.

FRT-mediated deletion. Two transposons carrying FRT elements, *P{XP=FRT}d00445* and *PBac{WH=FRT}f02085*, were used for site-specific deletion of the *eps15* locus as described previously (Parks et al., 2004). In brief, second chromosomes containing both transposons were placed in trans with each other in a genetic background containing *P{ry*$^{+t7.2}$*=hsFLP}12* (Bloomington Stock Center). 1-h 37°C heat-shock treatments were given to the larvae on three consecutive days to induce expression of the FLP recombinase. *P{ry*$^{+t7.2}$*=hsFLP}12,* y^1*w*; P{XP=FRT}d00445/PBac{WH=FRT}f02085* females were then crossed to y^1*w*; L/CyO*. In the next generation, dark-eyed males were isolated as putative recombinants and were crossed to $eps15^{e75}$ to test for noncomplementation of lethality, leading to the isolation of the $eps15^{\Delta 29}$ allele. About 80% of the dark-eyed males failed to complement $eps15^{e75}$. PCR and sequencing showed that the junctions of *P{XP=FRT}d00445* and *PBac{WH=FRT}f0208* with their respective flanking DNA in the *eps15* locus were retained in homozygous $eps15^{\Delta 29}$ larvae, confirming recombination.

Genomic rescue construct. 10.8 kb of genomic DNA containing the wild-type *eps15* (2R region bp: 19811150–19821904; Berkeley *Drosophila* Genome Project release 3 [http://www.fruitfly.org/cgi-bin/annot/gbrowse]) was recovered from BAC RP98-3B7 (BACPAC Resources) by gap repair in the vector, 2.2B-1 P{acman} (Venken et al., 2006). In brief, we cloned 500-bp left and right homology arms separated by a BamHI site in P{acman}. The vector was linearized using BamHI and transformed into recombination-competent DH10B bacteria containing both BACRP98-3B7 and mini-λ-Tet (Court et al., 2003; Liu et al., 2003). Gap-repaired vectors were selected with Amp, screened by PCR, and verified by restriction enzyme digestion and sequencing. As a third chromosome insertion of this genomic construct, *P{Eps15-S}3-2-2-5b*, does not rescue homozygous $eps15^{e75}$ mutants, we maintain $eps15^{e75}$*; P{Eps15-S}3-2-2-5b* as a balanced line over a compound chromosome consisting of chromosomes 2 and 3. We then cross this line to $eps15^{\Delta 29}$ and *Df(2R)Dll-MP* to test for rescue of lethality. The presence of the *eps15* lesions was verified by homozygous lethality of the parental $eps15^{\Delta 29}$ and *Df(2R)Dll-MP* stocks used for the final rescue cross.

cDNA rescue constructs. Full-length Eps15 (Eps15wt), EHmut (full length with W54A, W174A, and W356A substitutions in the EH domains), and ΔDPF (residues 1–639) were subcloned from SD09478 cDNA into pUAST (Brand and Perrimon, 1993). *eps15* cDNAs were driven by one of the *elav*-based neuronal drivers, the $elav^{C155\text{-}Gal4}$ enhancer trap in the *elav* locus (Lin and Goodman, 1994), or an *elav* promoter::Gal4 fusion transgene (*elav-Gal4*^{3A4}) inserted in the third chromosome (Luo et al., 1994). The $elav^{C155\text{-}Gal4}$ driver drove higher transgene expression levels and rescued the lethality of $eps15^{e75}/eps15^{\Delta 29}$ more effectively than the third chromosome *elav-Gal4* driver. Rescue of *eps15* mutants was only observed when $elav^{C155\text{-}Gal4}$ or *elav-Gal4*^{3A4} was introduced in the same fly as the UAS-cDNA constructs. Presence of *eps15* lesions in rescue individuals was verified by lethality associated with homozygosity on the second chromosome in the parental lines, $eps15^{e75}$*; UAS-cDNA*, $eps15^{\Delta 29}$*; elav-Gal4*^{3A4}, and *C155;* $eps15^{\Delta 29}$.

Larval culture

Mutant larvae were separated from larvae bearing balancer chromosomes and cultured on grape juice agar with yeast paste (Loewen et al., 2001). This allows lethal phase of mutants to be determined without complications from overcrowding and competition from larvae bearing balancer chromosomes.

Immunohistochemistry and quantification of fluorescent images

Labeling of third instar NMJs, third instar brains, and adult brains was performed as described by Verstreken et al. (2003). Animals were dissected in PBS and fixed in 4% formaldehyde in PBS for 20 min. Tissue was extensively washed in PBS and permeabilized with 0.4% Triton X-100; for anti-endophilin labeling, permeabilization was performed using 0.1% Tween 20. Antibodies were used in the following dilutions: affinity-purified anti-Dap160, 1:500 (Roos and Kelly, 1998); mouse anti-Dlg, 1:150 (4F3; Parnas et al., 2001); rabbit anti-Dlg, 1:2,000 (Cho et al., 2000); guinea pig anti-Dlg, 1:500 (Parmentier et al., 2000); rabbit anti-HRP, 1:1,500 (Jackson ImmunoResearch Laboratories); rabbit anti–Stoned B, 1:200 (Andrews et al., 1996); mouse anti-Csp mAb 49, 1:20 (Zinsmaier et al., 1994); rat anti-Nwk, 1:500 (Coyle et al., 2004); rabbit anti-dynamin, 1:500 (Roos and Kelly, 1998); mouse anti-dynamin, 1:50 (clone 41; BD Biosciences); rabbit anti–α-adaptin, 1:50 (González-Gaitán and Jäckle, 1997); mouse anti–Fas II 1D4 guinea pig anti-endophilin, 1:200 (Verstreken et al., 2002); mouse anti-Bruchpilot nc82, 1:100 (Wagh et al., 2006); and anti–synaptotagmin I, 1:500 (Littleton et al., 1993, 1994). Secondary antibodies conjugated to Cy3 or Cy5 (Jackson ImmunoResearch Laboratories) or Alexa 488 or 594 (Invitrogen) were used at 1:250. Samples were mounted in Vectashield mounting medium (Vector Laboratories). For Fig. 2 (A, B, and E), Fig. 4, Fig. 8, and Fig. S1, images were captured with a confocal microscope (LSM 510; Carl Zeiss MicroImaging, Inc.) with a 40×/1.3 differential interference contrast plan-Neofluar oil-immersion lens using the LSM 5 software (Carl Zeiss MicroImaging, Inc.) and were processed using Amira 2.2 (Mercury Computer Systems) followed by Photoshop (Adobe). For Fig. 2 (C and D) and Fig. S2, images were viewed using a confocal system (MRC-1024; Bio-Rad Laboratories) mounted on a microscope (Eclipse E800; Nikon) and were captured using a 40×/1.3 NA or 60×/1.4 NA oil-immersion objective and LaserSharp software (Bio-Rad Laboratories). Brightness and contrast levels and color channels were adjusted using ImageJ (http://rsb.info.nih.gov/ij) or Photoshop.

For quantification of synaptic proteins, anti-Dlg labeling was used to outline type I boutons for quantification of synaptic protein levels (Lahey et al., 1994). Boutons on muscle 12 were scanned with *z* steps of 0.7 μm. Using Amira software, the Dlg-stained type I boutons in each confocal slice were highlighted, and the mean pixel intensity of all slices of the highlighted boutons of each muscle 12 NMJ were computed. Background fluorescence in muscle areas adjacent to the boutons was quantified similarly, and the background was subtracted from the bouton values to yield the mean intensity

of labeling in the boutons. The mean value from at least three mutant NMJs was then expressed as a percentage of the corresponding control value. The primary antibodies against presynaptic proteins were used at concentrations that produced strong specific labeling in the NMJ boutons without giving excessive background labeling in other tissues.

Biochemistry

Immunoprecipitation experiments were performed essentially as described previously (Bean et al., 2000; Verstreken et al., 2003). The Dap160 band was detected by in-gel trypsin digest followed by peptide determination using a Q-STAR hybrid tandem mass spectrometer (MDS Sciex). Spectra were searched against a NCBI nonredundant database with MASCOT MS/MS Ions search (Matrix Science). The only other two Coomassie blue–stained bands that were successfully identified were keratin (likely a contaminant from the experimenter) and CG5214, a mitochondrial enzyme in the tricarboxylic acid cycle. For Western blots, rabbit anti-Eps15 was used at 1:2,500, rabbit anti–α-adaptin (Dornan et al., 1997) at 1:200, rabbit anti-dynamin (Roos and Kelly, 1998) at 1:300, and rabbit anti-Dap160 (Roos and Kelly, 1998) at 1:500. For pull-down assays, Histidine (His)-tagged and GST fusion proteins were expressed in BL21(DE3)pLysS (Novagen) cells and purified from soluble fraction using Ni-NTA (QIAGEN) and glutathione (GE Healthcare) beads, respectively, before being used for binding assays. Ni-NTA agarose-coupled His-tagged UIM region of Eps15 (amino acids 1177–1253) was incubated with GST or GST-Ubiquitin (G76A; Lloyd et al., 2002) for 2 h at 4°C, washed extensively in PBS (0.01 M phosphate buffer, 0.0027 M KCl, and 0.137 M NaCl, pH 7.4) supplemented with 0.1% Triton X-100 and Complete protein inhibitor cocktail (Roche) and prepared for electrophoresis. For pull downs from fly head extracts, glutathione Sepharose–coupled GST, GST-3xEH (amino acides 1–403), and the GST-DPF region of Eps15 (amino acids 551–1001) were incubated with extracts (frozen heads homogenized in PBS supplemented with 2 mM $CaCl_2$, 1.5 mM $MgCl_2$, 1% Triton X-100, and Complete protein inhibitor cocktail; cleared soluble fraction adjusted to 0.1% Triton X-100 concentration) for 2 h at 4°C, washed extensively in the same buffer, and prepared for electrophoresis.

Electrophysiology and FM1-43FX uptake assay

Third instar electrophysiology was also performed essentially as described previously (Verstreken et al., 2002, 2003). Larvae were dissected, and recordings were performed in modified HL3: 110 mM NaCl; 5 mM KCl; 10 mM $NaHCO_3$; 5 mM Hepes; 30 mM sucrose; 5 mM trehalose; 10 mM $MgCl_2$; and 0, 0.5, or 5 mM $CaCl_2$ (as indicated in the text and figure legends). For 10-Hz stimulations, the above medium was modified to contain 4 mM $MgCl_2$ and 5 mM $CaCl_2$. Recordings of low-frequency stimulations and 10-Hz stimulations were made from muscles with resting potential lower than −60 and −65 mV, respectively.

For the FM1-43FX (Invitrogen) styryl dye uptake experiments, larvae were dissected on Sylgard plates and incubated in modified HL3 with 4 μM FM1-43FX, 5 mM $CaCl_2$, 90 mM KCl, and 25 mM NaCl for 10 min. Excess dye was then washed away with zero Ca^{2+} solution for 10–15 min, and labeling was imaged using a 40×/0.75w Acroplan water-immersion lens on the LSM 510 confocal microscope. Data acquisition as well as data processing and quantification were performed as described previously (Verstreken et al., 2003). The FM1-43FX dye uptake assay in Fig. 8 was performed as above, but the data were acquired after fixation with 4% formaldehyde in PBS, imaged using a 60×/1.4 NA oil-immersion objective on the MRC-1024 confocal system, and quantified using NIH ImageJ. Data acquired using the two methods were comparable. All electrophysiology and FM1-43FX uptake was performed at room temperature (~21–23°C), except when indicated otherwise.

TEM

Larval fillets were prepared in HL3 without Ca^{2+} and fixed in 4% paraformaldehyde/1% glutaraldehyde/0.1 M cacodylic acid, pH 7.2, or 3% paraformaldehyde/0.5% glutaraldehyde/0.1 M cacodylic acid, pH 7.2. Samples were postfixed in 2% OsO_4 and stained in 2% uranyl acetate, dehydrated in alcohol, and embedded in Spurr's resin (Electron Microscopy Sciences) or Durcupan (Fluka). Ultrathin sections were cut with a diamond knife (Diatome) and stained with 2% uranyl acetate and lead citrate on grids. The grids were then visualized with an electron microscope (JEM-1010; JEOL) fitted with a charge-coupled device digital camera (Gatan). To study the morphology of stimulated boutons, larval fillets were incubated in HL3 with 5 mM Ca^{2+} and 60 or 90 mM K^+ for 10 min and fixed immediately. In stimulation-recovery experiments, stimulated NMJs were allowed to recover for 1 min in normal HL3 without Ca^{2+} before fixation. Images were quantified by NIH ImageJ.

Preembedding immunocytochemistry

Muscles 6 and 7 were dissected from third instar *Drosophila* larvae were fixed in 4% paraformaldehyde and embedded in agarose (Sigma-Aldrich). Vibratome slices of the agarose blocks were incubated with guinea pig anti-Eps15 antiserum followed by secondary antibodies conjugated to 1.4-nm gold particles (Nanoprobes, Inc.). The immunogold labeling was silver enhanced using IntenSE Silver Enhancement kit (GE Healthcare), and samples were embedded in Durcupan ACM (Fluka) for ultrathin sectioning. Serial ultrathin sections were counterstained with uranyl acetate and lead citrate and examined in a microscope (Tecnai 12; FEI Company). Images were quantified using NIH ImageJ, and statistical evaluation was performed using Excel (Microsoft). Note that the silver enhancement technique works by the precipitation of silver particles around the gold particles, resulting in the formation of irregularly shaped black precipitates.

Online supplemental material

Fig. S1 illustrates the domain structure of *Drosophila* Eps15 and shows that the *eps15*-null alleles do not express detectable amounts of Eps15. Fig. S2 shows that mBSA endocytosis and dynamin levels are both normal in *eps15*-null hemocytes. Fig. S3 shows that dynamin and Dap160 levels are not substantially altered in the larval brains of *eps15* mutants. Fig. S4 shows that the EH, DPF, and UIM domains of Eps15 bind to Dap160, α-adaptin, and ubiquitin, respectively. Table S1 shows mass spectroscopy data of peptide sequences corresponding to Dap160, which coimmunoprecipitated with Eps15 (Fig. 1 A). Online supplemental material is available at http://www.jcb.org/cgi/content/full/jcb.200701030/DC1.

We are grateful to C.-K. Yao for critical assessment of data on bouton morphology, and we thank H. McMahon for mass spectroscopy, Y.-T. Lei for quantification of morphological data, N. Tomilin for expert advice in EM, and K.S. Krishnan and A. Majumdar for sharing results and reagents before publication. In addition, we are grateful to K.W. Cho, R. Kelly, L. Kelly, B. Ganetzky, M. González-Gaitán, E. Buchner, and A. Jackson for antibodies; D. Court for mini-λ-Tet; and P. Verstreken, A. Fayyazudin, and C. Ly for critical comments on this manuscript.

We acknowledge stocks and antibodies from the Bloomington and Szeged *Drosophila* stock centers and the Developmental Biology Hybridoma Center, Iowa. Confocal microscopy was supported by the Mental Retardation and Developmental Disabilities Research Center. T.-W. Koh acknowledges support from the Baylor College of Medicine–Karolinska Institutet Exchange Program. Y.P. Wairkar was supported by a Nehru scholarship from the Cambridge Commonwealth Trust. This work was supported by a grant (8/C19002) and a Research Development Fellowship from the Biotechnology and Biological Sciences Research Council to C.J. O'Kane, a Career Development Award (G120/414) from the Medical Research Council to I.M. Robinson, fellowship from Hjärnfonden to E. Evergren, The Swedish Research Council (13473) and Fernströms Stiftelse to O. Shupliakov, and a Howard Hughes Institutional Grant (76200-549202) to I.M. Robinson. H.J. Bellen is supported by the Howard Hughes Medical Institute.

Submitted: 5 January 2007
Accepted: 18 June 2007

References

Andrews, J., M. Smith, J. Merakovsky, M. Coulson, F. Hannan, and L.E. Kelly. 1996. The stoned locus of *Drosophila melanogaster* produces a dicistronic transcript and encodes two distinct polypeptides. *Genetics.* 143:1699–1711.

Bache, K.G., C. Raiborg, A. Mehlum, and H. Stenmark. 2003. STAM and Hrs are subunits of a multivalent ubiquitin-binding complex on early endosomes. *J. Biol. Chem.* 278:12513–12521.

Bean, A.J., S. Davanger, M.F. Chou, B. Gerhardt, S. Tsujimoto, and Y. Chang. 2000. Hrs-2 regulates receptor-mediated endocytosis via interactions with Eps15. *J. Biol. Chem.* 275:15271–15278.

Bellen, H.J., and V. Budnik. 2000. The neuromuscular junction. *In Drosophila* Protocols. W. Sullivan, M. Ashburner, and R.S. Hawley, editors. Cold Spring Harbor Laboratory Press, Cold Spring Harbor, NY. 175–199.

Benmerah, A., C. Lamaze, B. Begue, S.L. Schmid, A. Dautry-Varsat, and N. Cerf-Bensussan. 1998. AP-2/Eps15 interaction is required for receptor-mediated endocytosis. *J. Cell Biol.* 140:1055–1062.

Benmerah, A., M. Bayrou, N. Cerf-Bensussan, and A. Dautry-Varsat. 1999. Inhibition of clathrin-coated pit assembly by an Eps15 mutant. *J. Cell Sci.* 112:1303–1311.

Brand, A.H., and N. Perrimon. 1993. Targeted gene expression as a means of altering cell fates and generating dominant phenotypes. *Development.* 118:401–415.

Broadie, K. 2004. Synapse scaffolding: intersection of endocytosis and growth. *Curr. Biol.* 14:R853–R855.

Carbone, R., S. Fre, G. Iannolo, F. Belleudi, P. Mancini, P.G. Pelicci, M.R. Torrisi, and P.P. Di Fiore. 1997. eps15 and eps15R are essential components of the endocytic pathway. *Cancer Res.* 57:5498–5504.

Cho, K.O., J. Chern, S. Izaddoost, and K.W. Choi. 2000. Novel signaling from the peripodial membrane is essential for eye disc patterning in *Drosophila*. *Cell.* 103:331–342.

Cohen, S.M., G. Bronner, F. Kuttner, G. Jurgens, and H. Jackle. 1989. Distalless encodes a homoeodomain protein required for limb development in *Drosophila*. *Nature*. 338: 432–434.

Court, D.L., S. Swaminathan, D. Yu, H. Wilson, T. Baker, M. Bubunenko, J. Sawitzke, and S.K. Sharan. 2003. Mini-lambda: a tractable system for chromosome and BAC engineering. *Gene.* 315:63–69.

Coyle, I.P., Y.H. Koh, W.C. Lee, J. Slind, T. Fergestad, J.T. Littleton, and B. Ganetzky. 2004. Nervous wreck, an SH3 adaptor protein that interacts with Wsp, regulates synaptic growth in *Drosophila*. *Neuron.* 41:521–534.

Diril, M.K., M. Wienisch, N. Jung, J. Klingauf, and V. Haucke. 2006. Stonin 2 is an AP-2-dependent endocytic sorting adaptor for synaptotagmin internalization and recycling. *Dev. Cell.* 10:233–244.

Dornan, S., A.P. Jackson, and N.J. Gay. 1997. Alpha-adaptin, a marker for endocytosis, is expressed in complex patterns during *Drosophila* development. *Mol. Biol. Cell.* 8:1391–1403.

Duncan, M.C., M.J. Cope, B.L. Goode, B. Wendland, and D.G. Drubin. 2001. Yeast Eps15-like endocytic protein, Pan1p, activates the Arp2/3 complex. *Nat. Cell Biol.* 3:687–690.

Eaton, B.A., R.D. Fetter, and G.W. Davis. 2002. Dynactin is necessary for synapse stabilization. *Neuron.* 34:729–741.

Estes, P.S., J. Roos, A. van der Bliek, R.B. Kelly, K.S. Krishnan, and M. Ramaswami. 1996. Traffic of dynamin within individual *Drosophila* synaptic boutons relative to compartment-specific markers. *J. Neurosci.* 16:5443–5456.

Evergren, E., H. Gad, K. Walther, A. Sundborger, N. Tomilin, and O. Shupliakov. 2007. Intersectin is a negative regulator of dynamin recruitment to the synaptic endocytic zone in the central synapse. *J. Neurosci.* 27:379–390.

Fazioli, F., L. Minichiello, B. Matoskova, W.T. Wong, and P.P. Di Fiore. 1993. eps15, a novel tyrosine kinase substrate, exhibits transforming activity. *Mol. Cell. Biol.* 13:5814–5828.

Fergestad, T., and K. Broadie. 2001. Interaction of stoned and synaptotagmin in synaptic vesicle endocytosis. *J. Neurosci.* 21:1218–1227.

Fernandez-Chacon, R., M. Achiriloaie, R. Janz, J.P. Albanesi, and T.C. Sudhof. 2000. SCAMP1 function in endocytosis. *J. Biol. Chem.* 275:12752–12756.

Gad, H., N. Ringstad, P. Low, O. Kjaerulff, J. Gustafsson, M. Wenk, G. Di Paolo, Y. Nemoto, J. Crun, M.H. Ellisman, et al. 2000. Fission and uncoating of synaptic clathrin-coated vesicles are perturbed by disruption of interactions with the SH3 domain of endophilin. *Neuron.* 27:301–312.

Gerlitz, O., D. Nellen, M. Ottiger, and K. Basler. 2002. A screen for genes expressed in *Drosophila* imaginal discs. *Int. J. Dev. Biol.* 46:173–176.

Golic, K.G. 1994. Local transposition of *P* elements in *Drosophila melanogaster* and recombination between duplicated elements using a site-specific recombinase. *Genetics.* 137:551–563.

González-Gaitán, M., and H. Jäckle. 1997. Role of *Drosophila* alpha-adaptin in presynaptic vesicle recycling. *Cell.* 88:767–776.

Granseth, B., B. Odermatt, S.J. Royle, and L. Lagnado. 2006. Clathrin-mediated endocytosis is the dominant mechanism of vesicle retrieval at hippocampal synapses. *Neuron.* 51:773–786.

Halfon, M.S., S. Gisselbrecht, J. Lu, B. Estrada, H. Keshishian, and A.M. Michelson. 2002. New fluorescent protein reporters for use with the *Drosophila* Gal4 expression system and for vital detection of balancer chromosomes. *Genesis.* 34:135–138.

He, L., X.S. Wu, R. Mohan, and L.G. Wu. 2006. Two modes of fusion pore opening revealed by cell-attached recordings at a synapse. *Nature.* 444:102–105.

Irie, F., and Y. Yamaguchi. 2002. EphB receptors regulate dendritic spine development via intersectin, Cdc42 and N-WASP. *Nat. Neurosci.* 5:1117–1118.

Itoh, T., K.S. Erdmann, A. Roux, B. Habermann, H. Werner, and P. De Camilli. 2005. Dynamin and the actin cytoskeleton cooperatively regulate plasma membrane invagination by BAR and F-BAR proteins. *Dev. Cell.* 9:791–804.

Jarousse, N., J.D. Wilson, D. Arac, J. Rizo, and R.B. Kelly. 2003. Endocytosis of synaptotagmin 1 is mediated by a novel, tryptophan-containing motif. *Traffic.* 4:468–478.

Koenig, J.H., and K. Ikeda. 1989. Disappearance and reformation of synaptic vesicle membrane upon transmitter release observed under reversible blockage of membrane retrieval. *J. Neurosci.* 9:3844–3860.

Koenig, J.H., and K. Ikeda. 1996. Synaptic vesicles have two distinct recycling pathways. *J. Cell Biol.* 135:797–808.

Koenig, J.H., and K. Ikeda. 1999. Contribution of active zone subpopulation of vesicles to evoked and spontaneous release. *J. Neurophysiol.* 81:1495–1505.

Koenig, J.H., K. Yamaoka, and K. Ikeda. 1993. Calcium-induced translocation of synaptic vesicles to the active site. *J. Neurosci.* 13:2313–2322.

Koh, T.W., P. Verstreken, and H.J. Bellen. 2004. Dap160/intersectin acts as a stabilizing scaffold required for synaptic development and vesicle endocytosis. *Neuron.* 43:193–205.

Kosaka, T., and K. Ikeda. 1983. Possible temperature-dependent blockage of synaptic vesicle recycling induced by a single gene mutation in *Drosophila*. *J. Neurobiol.* 14:207–225.

Lahey, T., M. Gorczyca, X.X. Jia, and V. Budnik. 1994. The *Drosophila* tumor suppressor gene *dlg* is required for normal synaptic bouton structure. *Neuron.* 13:823–835.

Lin, D.M., and C.S. Goodman. 1994. Ectopic and increased expression of Fasciclin II alters motoneuron growth cone guidance. *Neuron.* 13:507–523.

Littleton, J.T., M. Stern, K. Schulze, M. Perin, and H.J. Bellen. 1993. Mutational analysis of *Drosophila synaptotagmin* demonstrates its essential role in Ca(2+)-activated neurotransmitter release. *Cell.* 74:1125–1134.

Littleton, J.T., M. Stern, M. Perin, and H.J. Bellen. 1994. Calcium dependence of neurotransmitter release and rate of spontaneous vesicle fusions are altered in *Drosophila* synaptotagmin mutants. *Proc. Natl. Acad. Sci. USA.* 91:10888–10892.

Liu, P., N.A. Jenkins, and N.G. Copeland. 2003. A highly efficient recombineering-based method for generating conditional knockout mutations. *Genome Res.* 13:476–484.

Lloyd, T.E., P. Verstreken, E.J. Ostrin, A. Phillippi, O. Lichtarge, and H.J. Bellen. 2000. A genome-wide search for synaptic vesicle cycle proteins in *Drosophila*. *Neuron.* 26:45–50.

Lloyd, T.E., R. Atkinson, M.N. Wu, Y. Zhou, G. Pennetta, and H.J. Bellen. 2002. Hrs regulates endosome membrane invagination and tyrosine kinase receptor signaling in *Drosophila*. *Cell.* 108:261–269.

Loewen, C.A., J.M. Mackler, and N.E. Reist. 2001. *Drosophila synaptotagmin I* null mutants survive to early adulthood. *Genesis.* 31:30–36.

Luo, L., Y.J. Liao, L.Y. Jan, and Y.N. Jan. 1994. Distinct morphogenetic functions of similar small GTPases: *Drosophila* Drac1 is involved in axonal outgrowth and myoblast fusion. *Genes Dev.* 8:1787–1802.

Majumdar, A., S. Ramagiri, and R. Rikhy. 2006. *Drosophila* homologue of Eps15 is essential for synaptic vesicle recycling. *Exp. Cell Res.* 312:2288–2298.

Marie, B., S.T. Sweeney, K.E. Poskanzer, J. Roos, R.B. Kelly, and G.W. Davis. 2004. Dap160/intersectin scaffolds the periactive zone to achieve high-fidelity endocytosis and normal synaptic growth. *Neuron.* 43:207–219.

Martina, J.A., C.J. Bonangelino, R.C. Aguilar, and J.S. Bonifacino. 2001. Stonin 2: an adaptor-like protein that interacts with components of the endocytic machinery. *J. Cell Biol.* 153:1111–1120.

McPherson, P.S. 2002. The endocytic machinery at an interface with the actin cytoskeleton: a dynamic, hip intersection. *Trends Cell Biol.* 12:312–315.

Merrifield, C.J., M.E. Feldman, L. Wan, and W. Almers. 2002. Imaging actin and dynamin recruitment during invagination of single clathrin-coated pits. *Nat. Cell Biol.* 4:691–698.

Morgan, J.R., K. Prasad, S. Jin, G.J. Augustine, and E.M. Lafer. 2003. Eps15 homology domain-NPF motif interactions regulate clathrin coat assembly during synaptic vesicle recycling. *J. Biol. Chem.* 278:33583–33592.

Motley, A.M., N. Berg, M.J. Taylor, D.A. Sahlender, J. Hirst, D.J. Owen, and M.S. Robinson. 2006. Functional analysis of AP-2 α and μ2 subunits. *Mol. Biol. Cell.* 17:5298–5308.

Parks, A.L., K.R. Cook, M. Belvin, N.A. Dompe, R. Fawcett, K. Huppert, L.R. Tan, C.G. Winter, K.P. Bogart, J.E. Deal, et al. 2004. Systematic generation of high-resolution deletion coverage of the *Drosophila melanogaster* genome. *Nat. Genet.* 36:288–292.

Parmentier, M.L., D. Woods, S. Greig, P.G. Phan, A. Radovic, P. Bryant, and C.J. O'Kane. 2000. Rapsynoid/partner of inscuteable controls asymmetric division of larval neuroblasts in *Drosophila*. *J. Neurosci.* 20:RC84.

Parnas, D., A.P. Haghighi, R.D. Fetter, S.W. Kim, and C.S. Goodman. 2001. Regulation of postsynaptic structure and protein localization by the Rho-type guanine nucleotide exchange factor dPix. *Neuron.* 32:415–424.

Pennetta, G., P. Hiesinger, R. Fabian-Fine, I. Meinertzhagen, and H. Bellen. 2002. *Drosophila* VAP-33A directs bouton formation at neuromuscular junctions in a dosage-dependent manner. *Neuron.* 35:291–306.

Polo, S., S. Sigismund, M. Faretta, M. Guidi, M.R. Capua, G. Bossi, H. Chen, P. De Camilli, and P.P. Di Fiore. 2002. A single motif responsible for

ubiquitin recognition and monoubiquitination in endocytic proteins. *Nature.* 416:451–455.

Polo, S., S. Confalonieri, A.E. Salcini, and P.P. Di Fiore. 2003. EH and UIM: endocytosis and more. *Sci. STKE.* 2003:re17.

Poskanzer, K.E., K.W. Marek, S.T. Sweeney, and G.W. Davis. 2003. Synaptotagmin I is necessary for compensatory synaptic vesicle endocytosis in vivo. *Nature.* 426:559–563.

Roos, J., and R.B. Kelly. 1998. Dap160, a neural-specific Eps15 homology and multiple SH3 domain-containing protein that interacts with *Drosophila* dynamin. *J. Biol. Chem.* 273:19108–19119.

Roos, J., and R.B. Kelly. 1999. The endocytic machinery in nerve terminals surrounds sites of exocytosis. *Curr. Biol.* 9:1411–1414.

Rørth, P. 1996. A modular misexpression screen in *Drosophila* detecting tissue-specific phenotypes. *Proc. Natl. Acad. Sci. USA.* 93:12418–12422.

Royle, S.J., and L. Lagnado. 2003. Endocytosis at the synaptic terminal. *J. Physiol.* 553:345–355.

Salcini, A.E., M.A. Hilliard, A. Croce, S. Arbucci, P. Luzzi, C. Tacchetti, L. Daniell, P. De Camilli, P.G. Pelicci, P.P. Di Fiore, and P. Bazzicalupo. 2001. The Eps15 *C. elegans* homologue EHS-1 is implicated in synaptic vesicle recycling. *Nat. Cell Biol.* 3:755–760.

Santolini, E., A.E. Salcini, B.K. Kay, M. Yamabhai, and P.P. Di Fiore. 1999. The EH network. *Exp. Cell Res.* 253:186–209.

Schuster, C.M., G.W. Davis, R.D. Fetter, and C.S. Goodman. 1996. Genetic dissection of structural and functional components of synaptic plasticity. I. Fasciclin II controls synaptic stabilization and growth. *Neuron.* 17:641–654.

Sengar, A.S., W. Wang, J. Bishay, S. Cohen, and S.E. Egan. 1999. The EH and SH3 domain Ese proteins regulate endocytosis by linking to dynamin and Eps15. *EMBO J.* 18:1159–1171.

Shupliakov, O., P. Low, D. Grabs, H. Gad, H. Chen, C. David, K. Takei, P. De Camilli, and L. Brodin. 1997. Synaptic vesicle endocytosis impaired by disruption of dynamin-SH3 domain interactions. *Science.* 276:259–263.

Shupliakov, O., O. Bloom, J.S. Gustafsson, O. Kjaerulff, P. Low, N. Tomilin, V.A. Pieribone, P. Greengard, and L. Brodin. 2002. Impaired recycling of synaptic vesicles after acute perturbation of the presynaptic actin cytoskeleton. *Proc. Natl. Acad. Sci. USA.* 99:14476–14481.

Sigismund, S., T. Woelk, C. Puri, E. Maspero, C. Tacchetti, P. Transidico, P.P. Di Fiore, and S. Polo. 2005. Clathrin-independent endocytosis of ubiquitinated cargos. *Proc. Natl. Acad. Sci. USA.* 102:2760–2765.

Stowell, M.H., B. Marks, P. Wigge, and H.T. McMahon. 1999. Nucleotide-dependent conformational changes in dynamin: evidence for a mechanochemical molecular spring. *Nat. Cell Biol.* 1:27–32.

Sun, J.Y., X.S. Wu, and L.G. Wu. 2002. Single and multiple vesicle fusion induce different rates of endocytosis at a central synapse. *Nature.* 417:555–559.

Takei, K., V. Haucke, V. Slepnev, K. Farsad, M. Salazar, H. Chen, and P. De Camilli. 1998. Generation of coated intermediates of clathrin-mediated endocytosis on protein-free liposomes. *Cell.* 94:131–141.

Tang, H.Y., and M. Cai. 1996. The EH-domain-containing protein Pan1 is required for normal organization of the actin cytoskeleton in *Saccharomyces cerevisiae*. *Mol. Cell. Biol.* 16:4897–4914.

Tebar, F., T. Sorkina, A. Sorkin, M. Ericsson, and T. Kirchhausen. 1996. Eps15 is a component of clathrin-coated pits and vesicles and is located at the rim of coated pits. *J. Biol. Chem.* 271:28727–28730.

Teng, H., and R.S. Wilkinson. 2000. Clathrin-mediated endocytosis near active zones in snake motor boutons. *J. Neurosci.* 20:7986–7993.

Thibault, S.T., M.A. Singer, W.Y. Miyazaki, B. Milash, N.A. Dompe, C.M. Singh, R. Buchholz, M. Demsky, R. Fawcett, H.L. Francis-Lang, et al. 2004. A complementary transposon tool kit for *Drosophila melanogaster* using P and piggyBac. *Nat. Genet.* 36:283–287.

Torrisi, M.R., L.V. Lotti, F. Belleudi, R. Gradini, A.E. Salcini, S. Confalonieri, P.G. Pelicci, and P.P. Di Fiore. 1999. Eps15 is recruited to the plasma membrane upon epidermal growth factor receptor activation and localizes to components of the endocytic pathway during receptor internalization. *Mol. Biol. Cell.* 10:417–434.

Tsujita, K., S. Suetsugu, N. Sasaki, M. Furutani, T. Oikawa, and T. Takenawa. 2006. Coordination between the actin cytoskeleton and membrane deformation by a novel membrane tubulation domain of PCH proteins is involved in endocytosis. *J. Cell Biol.* 172:269–279.

Venken, K.J., Y. He, R.A. Hoskins, and H.J. Bellen. 2006. P[acman]: a BAC transgenic platform for targeted insertion of large DNA fragments in *D. melanogaster*. *Science.* 314:1747–1751.

Verstreken, P., O. Kjaerulff, T.E. Lloyd, R. Atkinson, Y. Zhou, I.A. Meinertzhagen, and H.J. Bellen. 2002. Endophilin mutations block clathrin-mediated endocytosis but not neurotransmitter release. *Cell.* 109:101–112.

Verstreken, P., T.W. Koh, K.L. Schulze, R.G. Zhai, P.R. Hiesinger, Y. Zhou, S.Q. Mehta, Y. Cao, J. Roos, and H.J. Bellen. 2003. Synaptojanin is recruited by endophilin to promote synaptic vesicle uncoating. *Neuron.* 40:733–748.

Wagh, D.A., T.M. Rasse, E. Asan, A. Hofbauer, I. Schwenkert, H. Durrbeck, S. Buchner, M.C. Dabauvalle, M. Schmidt, G. Qin, et al. 2006. Bruchpilot, a protein with homology to ELKS/CAST, is required for structural integrity and function of synaptic active zones in *Drosophila*. *Neuron.* 49:833–844.

Wendland, B., J.M. McCaffery, Q. Xiao, and S.D. Emr. 1996. A novel fluorescence-activated cell sorter-based screen for yeast endocytosis mutants identifies a yeast homologue of mammalian eps15. *J. Cell Biol.* 135:1485–1500.

Wucherpfennig, T., M. Wilsch-Brauninger, and M. González-Gaitán. 2003. Role of *Drosophila* Rab5 during endosomal trafficking at the synapse and evoked neurotransmitter release. *J. Cell Biol.* 161:609–624.

Zamanian, J.L., and R.B. Kelly. 2003. Intersectin 1L guanine nucleotide exchange activity is regulated by adjacent src homology 3 domains that are also involved in endocytosis. *Mol. Biol. Cell.* 14:1624–1637.

Zinsmaier, K.E., K.K. Eberle, E. Buchner, N. Walter, and S. Benzer. 1994. Paralysis and early death in cysteine string protein mutants of *Drosophila*. *Science.* 263:977–980.